Sustainable Cities and Society 131 (2025) 106764

Contents lists available at ScienceDirect

Sustainable Cities and Society

journal homepage: www.elsevier.com/locate/scs

Towards carbon-neutral energy systems: A two-layer robust model for day-ahead scheduling of emission-aware microgrids

Yali Wang [a], Zeyi Fan [b,c,*], Yahya Z. Alharthi [d], Shoujun Huang [e], Seyed Amir Mansouri [f]

[a] School of Economics & Management, Changsha University of Science & Technology, Changsha 410114, China
[b] College of Management, Shenzhen University, Shenzhen 518055, China
[c] Faculty of Business, Lingnan University, Hong Kong 999007, China
[d] Department of Electrical Engineering, College of Engineering, University of Hafr Albatin, Hafr Al Batin 39524, Saudi Arabia
[e] International School of Business & Finance, Sun Yat-Sen University, Zhuhai 519082, China
[f] Department of Engineering Systems & Services, Faculty of Technology, Policy & Management, Delft University of Technology, Delft, The Netherlands

ARTICLE INFO

Keywords:
Smart Energy Systems
Carbon Footprint
Decarbonization
Robust Scheduling
Microgrids
Electric Vehicle Fleets

ABSTRACT

Microgrids equipped with distributed renewable energy resources, energy storage systems, controllable loads, and vehicle-to-grid (V2G) technologies have emerged as critical enablers for sustainable energy transitions. However, their effective integration into day-ahead electricity markets requires advanced decentralized coordination mechanisms that ensure both robust scheduling under uncertainty and the preservation of agent privacy. Hence, this paper introduces a two-layer optimization framework to coordinate residential and industrial microgrids with the distribution network operator (DNO), addressing economic, technical, and environmental objectives. The proposed model employs an enhanced alternating direction method of multipliers (ADMM) algorithm, which dynamically adjusts power exchange prices based on carbon tax rates. This approach incentivizes low-carbon operations while preserving the confidentiality of internal microgrid schedules. Residential and industrial microgrids perform day-ahead scheduling in the first layer by leveraging the flexible capacities of their diverse technologies. Subsequently, they submit their desired exchange plans for participation in the day-ahead electricity market to the DNO in the second layer, where the feasibility of their implementation is evaluated. The model was validated on a 123-bus electricity distribution network comprising 32 residential microgrids and 17 industrial microgrids. The results demonstrated its effectiveness, achieving a 12.19 % reduction in carbon emissions and a 11.24 % decrease in operational costs. Furthermore, the proposed enhanced ADMM reduced convergence time by 43.16 % compared to the standard ADMM, significantly expediting coordination among decentralized agents in day-ahead markets.

1. Introduction

1.1. Background & motivations

The global transition toward renewable energy sources has underscored the importance of decarbonizing the power sector (Perwez et al., 2025). With the increasing penetration of distributed renewable energy resources (RES), such as wind and solar, modern electricity grids are evolving into highly decentralized systems characterized by the active participation of various stakeholders, including residential and industrial microgrids (Ifaei et al., 2025). These stakeholders are equipped with flexible assets such as energy storage systems, plug-in electric vehicles (PEVs), and demand-side management capabilities are becoming active participants in energy markets (Fuchs et al., 2024). This shift presents both opportunities and challenges for DNOs, who must balance the technical and economic coordination of these entities with the overarching goals of grid reliability, cost minimization, and environmental sustainability (Costanzo et al., 2024).

Day-ahead electricity markets serve as a critical platform for scheduling energy transactions, enabling stakeholders to plan their energy consumption, generation, and exchange in advance. In this context, microgrids have emerged as key players due to their ability to locally generate and consume electricity, thus reducing dependence on the centralized grid. Nevertheless, the unique characteristics of microgrids, such as their reliance on intermittent renewable generation and the need for robust coordination, complicate their seamless integration into market mechanisms (Nawaz et al., 2022; Tsaousoglou et al., 2022).

* Corresponding author.
E-mail addresses: viki23332025@163.com (Z. Fan), s.mansouri@tudelft.nl, amir.mansouri24@gmail.com (S.A. Mansouri).

https://doi.org/10.1016/j.scs.2025.106764
Received 13 March 2025; Received in revised form 24 August 2025; Accepted 26 August 2025
Available online 27 August 2025

Nomenclature

Abbreviations

ADMM	Alternating Direction Method of Multipliers
CHP	Combined Heat and Power
DNO	Distribution Network Operator
EWH	Electric Water Heater
HVAC	Heating, Ventilation, and Air Conditioning
MILP	Mixed-Integer Linear Programming
PEV	Plug-in Electric Vehicle
PV	Photovoltaic
RES	Renewable Energy Sources
V2G	Vehicle-to-Grid
VPP	Virtual Power Plant

Sets

e	Set of storage systems
g	Set of gas turbines
i	Set of industrial microgrids
n/m	Set of network buses
r	Set of residential microgrids
s	Set of solar systems
t	Set of operation time slots
v	Set of Plug-in Electric Vehicles
w	Set of wind turbines

Scalars

$\alpha^{(.)}_{(.)\to(.)}$	Energy conversion factor
α^{Ar}/α^{Dp}	Energy level percentage at arrival / departure time (%)
Δt	Time gap (h)
Δl	Insulation thickness (m)
$\delta^{Water}/\delta^{Air}$	Discomfort factors
ε	Maximum allowable deviation for temperature (%)
φ	Thermal conductivity (W/mC^o)
κ	Heat transfer coefficient (W/m^{2}C^o)
μ_t^{Grid}	Emission factor of grid power (kg/kW)
S^{Base}	Base power (kVA)
ϑ	Thermal constant of water (kWh/kgC^o)
ξ	Thermal conductance of the building (%)
$Irradiance^{Max}$	Solar constant (W/m^2)

Parameters

$a_i/b_i/c_i/d_i/e_i/f_i$	Coefficients of gas consumption function of CHP
B_l/G_l	Susceptance / Conductance of branch (p.u)
$E_r^{Storage,0}$	Initial energy level of storage system (kWh)
$E_r^{Storage,Min}/E_r^{Storage,Max}$	Min / Max energy level of storage system (kWh)
$E_v^{PEV,Min}/E_v^{PEV,Max}$	Min / Max energy level of PEV (kWh)
$H_i^{(.)}$	CHP heat generation operating points (kW)
$H_i^{Boiler,Max}$	Boiler capacity (kW)
$Irradiance_t$	Solar irradiance (W/m^2)
$\kappa_{n,l}^{Flow}$	Power flow direction
λ_t^{Grid}	Price of power exchanges with the grid ($/kWh)
$\lambda_{r,t}^{Exch}/\lambda_{i,t}^{Exch}$	Price of power exchanges with microgrids ($/kWh)
$\lambda_r^{Storage}$	Operating cost of storage system ($/kWh)
$\lambda_r^{V2G}/\lambda_i^{V2G}$	Operation cost of V2G / G2V services ($/kWh)
λ_r^{Dev}	Price of final material ($/unit)
$\lambda_{i,t}^{Gas}$	Gas price ($/m^3)
$\lambda_g^{Turbine}$	Operating cost of gas turbine ($/kWh)
$M6_{i,t}^{P6,Desire}$	Desired final material (unit)
$M_i^{P1/P2/P3/P4/P5,Min}/M_i^{P1/P2/P3/P4/P5,Max}$	Min / Max storage capacity of materials (unit)
$M6_{i,t}^{P6,Min}/M6_{i,t}^{P6,Max}$	Min / Max storage capacity of final martial (unit)
$\mu_g^{Turbine}$	Emission factor of gas turbine (kg/kW)
$P_{r,t}^{Fixed}$	Fixed power of residential microgrid (kW)
$P_r^{Solar,Capacity}$	Solar system capacity (kW)
$P_r^{Charge,Max}/P_r^{Discharge,Max}$	Max charge / discharge level of storage system (kW)
$P_r^{Heater,Max}/P_i^{Heater,Max}$	Heater capacity (kW)
$P_r^{Conditioner,Max}$	HVAC capacity (kW)
$P_v^{G2V,Max}/P_v^{V2G,Max}$	Max charge / discharge level of PEV (kW)
$P_i^{(.)}$	CHP power generation operating points (kW)
$P_i^{Wind,Capacity}$	Wind turbine capacity (kW)
$P_g^{Turbine,Min}/P_g^{Turbine,Max}$	Min / Max active power capacity of gas turbine (kW)
$P_n^{Demand}/Q_n^{Demand}$	Active / Reactive load demand (kW / kVAR)
$P_{(.)}^{Exch,Min}/P_{(.)}^{Exch,Max}$	Power exchange limit for microgrids (kW)
$Q_g^{Turbine,Min}/Q_g^{Turbine,Max}$	Min / Max reactive power capacity of gas turbine (kVAR)
R_l	Resistance of branch (p.u)
ρ_r/ρ_i	Penalty factor of microgrids
R^{Dual}/R^{Primal}	Primal / Dual residuals
S_r^{Heater}	Surface area of the heater's tank (m^2)
$S_i^{M1/M2/M3/M4/M5/M6,0}$	Initial number of materials in warehouses (unit)
$T_{r,t}^{Water,Desire}$	Desired water temperature (C^o)
$T_{r,t}^{Air,Desire}$	Desired air temperature (C^o)
$T_r^{Water,0}$	Initial water temperature (C^o)
$T_{r,t}^{Air,0}$	Initial air temperature (C^o)
$T_{r,t}^{Water,Min}/T_{r,t}^{Water,Max}$	Min / Max water temperature (C^o)
$T_r^{Water,Cold}$	Cold water temperature (C^o)
$T_t^{Outside}$	Ambient temperature (C^o)
$T_r^{Air,Min}/T_r^{Air,Max}$	Min / Max air temperature (C^o)
$\theta_n^{Min}/\theta_n^{Max}$	Min / Max voltage angle (rad)
v_t	Wind speed (m/s)
$v_i^{CI}/v_i^{CO}/v_i^{R}$	Cut-in / Cut-Out / Rated wind speed (m/s)
Vol_n^{Min}/Vol_n^{Max}	Min / Max voltage magnitude (p.u)
ϖ^{Solar}	Solar system efficiency (%)
$\varpi^{Conditioner}$	HVAC efficiency (C^o/kWh)
$WI_{r,t}^{MG,Desire}$	Desired welfare index
$W_{r,t}^{Demand}$	Hot water demand (kg)

Variables

$Cost^{DNO}$	Operation cost of DNO ($)
$Cost_i^{MG}$	Operation cost of industrial microgrid ($)
$Cost_r^{MG}$	Operation cost of residential microgrid ($)
$\Delta M6_{i,t}$	Deviation of final material from its desired value (unit)
$E_{r,t}^{Storage}$	Energy level of storage system (kWh)
$E_{r,t}^{Heater}$	Required energy by water heater (kWh)
$E_{r,t}^{Heater,Loss}$	Energy loss of water heater (kWh)
$E_{v,t}^{PEV}$	Energy level of PEV (kWh)
$G_{i,t}^{CHP}$	CHP gas consumption (m^3)
$G_{i,t}^{Boiler}$	Boiler gas consumption (m^3)
$G_{i,t}^{(.)\to(.)}$	Gas flow between components in the industrial microgrid (m^3)
$G_{g,t}^{Turbine}$	Gas consumption of Gas turbine (m^3)
$H_{i,t}^{Charge}/H_{i,t}^{Discharge}$	Charge / Discharge heat of the storage system (kW)
$H_{i,t}^{CHP}$	CHP gas generation (kW)
$H_{i,t}^{Boiler}$	Boiler heat generation (kW)

$H_{i,t}^{Heater}$ Heat generation of electric heater (kW)
$H_{i,t}^{(.)\to(.)}$ Heat flow between components in the industrial microgrid (m^3)
$M6_{i,t}^{P6,Ch}$ Generated amount of final martial (unit)
$M_{i,t}^{P1/P2/P3/P4/P5,Ch}$ Generated amount of martials (unit)
$P_{(.),t}^{Charge}/P_{(.),t}^{Discharge}$ Charge / Discharge power of the storage system (kW)
$P_{r,t}^{Exch}$ Power exchange of residential microgrid (kW)
$P_{v,t}^{G2V}/P_{v,t}^{V2G}$ Charge / Discharge power of PEV (kW)
$P_{r,t}^{Variable}$ Power consumption of controllable loads (kW)
$P_{r,t}^{Heater}/P_{i,t}^{Heater}$ Power consumption of heaters (kW)
$P_{r,t}^{Conditioner}$ Power consumption of HVAC (kW)
$P_{i,t}^{(.)\to(.)}$ Power flow between components in the industrial microgrid (m^3)
P_{t}^{Grid} Power exchanges with the grid (kW)
$P_{g,t}^{Turbine}/Q_{g,t}^{Turbine}$ Gas turbine active / reactive power generation (kW / kVAR)
$P_{i,t}^{CHP}$ CHP power generation (kW)
$P_{(.),t}^{Solar}$ Solar system power generation (kW)
$P_{(.),t}^{Wind}$ Wind turbine power generation (kW)
$P_{l,t}^{Line}/Q_{l,t}^{Line}$ Active / Reactive power flow (kW / kVAR)
$S_{i,t}^{M1/M2/M3/M4/M5/M6}$ Stored number of materials in warehouses (unit)
$T_{r,t}^{Water}$ Water temperature (C^o)
$T_{r,t}^{Air}$ Air temperature (C^o)
$\theta_{n,t}$ Voltage angle (rad)
$Vol_{n,t}$ Voltage magnitude (rad)
$WI_{r,t}^{MG}$ Welfare index of microgrids

Binary Variables
$u_{i,t}^{CHP}$ Operation status of CHP
$u_{r,t}^{Charge}/u_{r,t}^{Discharge}$ Charging / discharging status of storage system
$u_{v,t}^{G2V}/u_{v,t}^{V2G}$ Charging / discharging status of PEV
$u_{i,t}^{I}/u_{i,t}^{II}$ Operation status of CHP zones

From an operational perspective, ensuring real-time feasibility of day-ahead schedules is paramount, particularly in renewable-energy-rich systems where uncertainties in generation and demand are inherent. Moreover, as environmental concerns gain prominence, electricity market mechanisms must incentivize emission reduction strategies. Despite these priorities, traditional centralized market frameworks often fall short in addressing the conflicting objectives of information security, cost minimization, and environmental sustainability, especially in decentralized settings (Cagnano et al., 2020; Sharma et al., 2022).

Motivated by these challenges, this study introduces an ADMM-based optimization framework for day-ahead scheduling of microgrids in decentralized electricity markets. The model ensures information privacy, facilitates coordination between microgrids and the DNO, and incorporates dynamic pricing and carbon taxation to align decisions with environmental objectives. This approach addresses the critical need for robust, emission-aware, and efficient market-aligned scheduling in renewable-energy-rich smart grids.

1.2. Related works

Over the past decade, extensive research has explored strategies for integrating decentralized agents into coordinated power and gas network operations within energy markets. In this context, (Ranjbar et al., 2024) proposes a bilevel optimization framework for coordinated power management between microgrids and a smart distribution network in day-ahead markets. It integrates centralized and decentralized layers to minimize energy costs, enhance operational efficiency, and improve flexibility under uncertainty. Results demonstrate up to 67 % energy loss reduction, 47 % voltage improvement, and 22 % cost savings, achieving nearly full flexibility. The authors in (Yan & Xu, 2023) propose a deep reinforcement learning framework for microgrid bidding in electricity markets, including reserve offers. Based on a Markov decision process, the method focuses on day-ahead market participation, using state-space models of distributed energy resources to train a policy network via deep deterministic policy gradient. The strategy is validated with real-world microgrid systems and Singapore spot market data. (Zou et al., 2023) introduces an energy management approach for multi-energy microgrids supplying electrical and thermal energy, leveraging the transactive energy concept. A Stackelberg game-theoretic bi-level optimization framework coordinates energy scheduling and pricing at the upper level with trading strategies of agents at the lower level. The model is reformulated into a single-level mixed-integer linear programming (MILP) for tractability, integrating adaptive stochastic optimization to address day-ahead and intra-day markets. Risk aversion is managed using the conditional value at risk (CvaR) method, while adaptive Progressive Hedging and outer approximation algorithms enhance computational efficiency. Simulations validate the method's effectiveness and algorithmic performance. The authors in (J. Wang et al., 2024) propose a stochastic bidding strategy for a renewable-powered microgrid in electricity, thermal, and hydrogen markets. A bi-level MILP model optimizes microgrid profits and incorporates market pricing, renewable uncertainties via chance constraints, and advanced energy technologies. Results demonstrate reduced curtailment, adaptive trading strategies, and enhanced economic benefits. The authors in (Alrasheedi et al., 2024) address the microgrid bidding strategy in day-ahead electricity markets using a smart predict-and-optimize (SPO) approach. Unlike accuracy-focused methods, the SPO method predicts real-time price intervals with a cost-oriented trilevel programming model. The problem is solved using a reformulation-and-decomposition algorithm, demonstrating improved cost efficiency for microgrids. (Silva-Rodriguez et al., 2024) proposes a light robust optimization framework for microgrid participation in day-ahead electricity markets, co-optimizing energy and reserves. The method introduces a tunable robustness parameter and three reserve formulations: fixed, uncertainty-based, and a combined approach. Results show the combined method reduces activation costs by up to 263 % while enhancing market efficiency and socio-economic welfare. The authors in (Chen et al., 2024) address microgrid participation in electricity and regulation markets, focusing on complementary synergy among diverse resources and microgrids. They propose a two-stage model for virtual power plants (VPPs) with day-ahead scheduling and real-time control, integrating an adaptive microgrid mechanism to optimize economic benefits and grid frequency stability. Results validate the approach, showcasing its effectiveness in maximizing VPP profitability and enhancing grid regulation capacity. (Y. Wang et al., 2023) introduces a day-ahead bidding strategy for regional microgrids in electricity markets, addressing uncertainties from renewable generation and multi-energy loads using a hybrid stochastic and chance-constrained programming approach. A gradient boosted regression tree method reformulates chance constraints into deterministic ones, optimizing bidding quantities and operational costs. Simulations in PJM and Guangdong markets validate the strategy's effectiveness. The study in (Herding et al., 2023) develops an optimal day-ahead market bidding strategy for a microgrid with batteries, generators, photovoltaic (PV) systems, and commercial loads. Unlike

existing methods, it integrates price selection into bidding curve optimization, adhering to market rules. Using a two-stage stochastic MILP model, the approach addresses uncertainties in electricity prices and PV generation, minimizing expected operational costs. Monte Carlo simulations validate its performance against deterministic and alternative stochastic strategies. (Y.P. Xu et al., 2022) presents a hybrid robust-stochastic optimization framework for scheduling multi-energy microgrids to minimize operational costs and emissions. The model integrates hydrogen-based technologies, energy conversion systems, and a hybrid demand response scheme, serving flexible and non-flexible loads like data centers. Applied to day-ahead markets, the strategy reduces costs by 8.2 % and emissions by 3.9 %, demonstrating its effectiveness. The work in (Mansouri et al., 2024) proposes a multilevel framework to enhance the integration of renewable energy and PEV fleets with microgrids. Leveraging flexible appliances, thermostatically controlled loads, and PEVs, it models smart residential buildings as virtual energy storage systems (VESS) and optimizes microgrid scheduling and market clearing using an adaptive ADMM algorithm. The approach reduces flexibility market costs by 49.67 %, network losses by 24.1 %, and improves voltage profiles, ensuring efficiency and privacy in local electricity markets. (Ma et al., 2018) proposes an online energy management algorithm for networked microgrids with high DER penetration to address power generation uncertainty. Using an online ADMM approach with past generation data, the algorithm delivers less conservative schedules than robust optimization. Numerical results validate its effectiveness. (Y. Xu et al., 2023) introduces a coordinated scheduling model for shared energy storage systems and multi-microgrids to address renewable energy's volatility. Using Nash bargaining, benefits are redistributed to ensure cooperation, while a two-layer ADMM algorithm protects data privacy. Simulations confirm the model's efficiency, the ADMM's effectiveness, and its potential to support sustainable cities.

In recent years, extensive research has concentrated on harnessing the potential of flexible demand-side resources to drive decarbonization and promote sustainable energy systems. The review in (Hossain Lipu et al., 2022) investigates the role of battery energy storage systems in decarbonizing microgrids, addressing challenges such as intermittencies, energy imbalances, and high costs. It explores optimization objectives for storage system, including cost, capacity, lifetime, and emissions, and classifies various scheduling controllers and algorithms based on frameworks, execution, and findings. The study highlights the impact of optimized energy storage scheduling on microgrid sustainability and provides recommendations for advancing resilient, cost-effective, and decarbonized microgrid operations. The work in (Hwang Goh et al., 2022) presents a comprehensive multi-stage energy optimization framework for microgrids under renewable energy uncertainty. Leveraging scenario analysis and quantum particle swarm optimization, the framework integrates carbon trading mechanisms and demand-side response strategies to enhance microgrid performance. Results highlight the dual benefits of reduced emissions through carbon trading policies and improved economic efficiency, with a 27.48 % increase in cost savings achieved via high demand-side participation. (Neri et al., 2023) introduces a MILP model to reduce greenhouse gas emissions through energy symbiosis in industrial districts. By optimizing inter-firm energy exchanges and integrating distributed renewable energy generators and battery energy storage systems, the model achieves an 84.59 % reduction in emissions and a 43.46 % cost savings over a one-year period. The study in (Shen et al., 2024) proposes a robust optimization model for microgrid operation, utilizing renewable energy forecasts and uncertainties with neural networks and an advanced algorithm. The approach reduces costs by 14.2 % compared to intra-day strategies, while carbon constraints favor gas turbines and energy storage. A balance is identified to optimize energy use, costs, and emissions. (Jin et al., 2024) proposes a co-scheduling model for power and waste heat in hydrogen microgrids, optimizing economic and environmental performance without thermal storage. Using the Improved Honey Badger Algorithm, the approach reduces costs by 16.47 % compared to conventional microgrids and 5.5 % over standard methods, demonstrating enhanced efficiency and sustainability. The authors in (Venkatesan et al., 2024) propose the SFO-CSGNN method for optimizing day-ahead microgrid scheduling, integrating PEVs and renewable energy. Combining Sunflower optimization for PEV scheduling and a graph neural network for performance prediction, the approach enhances reliability, flexibility, and sustainability, achieving superior cost savings over existing methods. (Li et al., 2024) proposes a robust energy scheduling model for off-grid electricity-heat microgrids, integrating carbon capture systems to achieve negative emissions. Using a chance-constrained approach, the model addresses uncertainties in wind power and emissions, optimizing costs, reserve capacity, and environmental impact. Simulations confirm its effectiveness. The authors in (Ali et al., 2023) address carbon emissions and operational costs in microgrids by coordinating PEVs and responsive loads to stabilize wind and photovoltaic variability. Using a two-phase framework and a modified sparrow search algorithm, the approach reduces emissions and enhances renewable integration, outperforming existing optimization methods. The work in (Bolurian et al., 2022) introduces a two-layer model for day-ahead microgrid scheduling, integrating energy storage, distributed generation, and demand-side management. Using C-Means clustering and column-and-constraint generation optimization, the model minimizes costs, emissions, and load variability under renewable and price uncertainties. Simulations confirm its efficiency over existing methods. The study in (Zhong et al., 2022) proposes an optimal energy management strategy for multi-energy multi-microgrid networks, balancing operation costs and carbon emissions. A two-phase approach is employed: day-ahead distributed scheduling ensures electricity sharing while preserving privacy, and intra-day scheduling minimizes adjustment and procurement costs using a rolling horizon method. Simulations confirm its effectiveness in reducing costs and emissions under renewable energy and demand uncertainties. (Zhang et al., 2024) developed a self-healing scheduling model using adaptive ADMM to coordinate smart prosumers under emergency conditions, although their study did not consider environmental aspects, carbon taxes, or energy pricing under normal operating conditions.

1.3. Research gaps and contributions

The literature review highlights several unresolved challenges in decentralized day-ahead scheduling of microgrids:

- **Gap 1:** Trade-off between privacy and optimality. Centralized methods can achieve global optimality but require agents to disclose sensitive internal data (e.g., cost coefficients, operational constraints, demand forecasts), undermining confidentiality. Hierarchical methods preserve privacy but cannot guarantee global optimality due to their sequential structure.
- **Gap 2:** Static treatment of carbon costs. Most existing works model carbon pricing as a fixed additional term in the objective function. This static approach does not dynamically influence agents' iterative decision-making, limiting its effectiveness in steering real-time low-carbon behavior.
- **Gap 3:** Lack of robust market participation under uncertainty. Prior studies often neglect the reliance of agents on costly spot markets when real-time deviations occur between forecasted and actual renewable generation or demand, leaving day-ahead schedules fragile to uncertainty.

This study bridges the identified gaps by proposing a comprehensive, distributed optimization framework that leverages advanced ADMM enhancements, integrates carbon taxes into pricing mechanisms, and embeds robust optimization techniques to ensure resilient, cost-effective, and environmentally aligned day-ahead market participation for DNOs and microgrids. The main contributions of this study are as

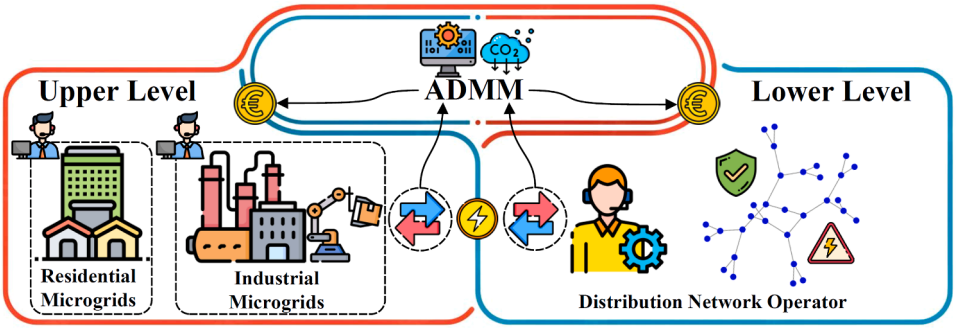

Fig. 1. Design of the two-layered model architecture.

follows:

- The proposed framework introduces a two-layer distributed optimization model to coordinate decentralized microgrids with DNOs in day-ahead electricity markets. In contrast to centralized methods, which can reach the global optimum but require agents to disclose sensitive internal data (e.g., cost functions, operational constraints, and demand forecasts), and hierarchical methods, which preserve privacy but fail to guarantee global optimality, our enhanced ADMM achieves both. It requires only the iterative exchange of coupling variables (power exchange schedules) while preserving all internal models locally. This structure ensures that agent confidentiality is fully maintained while convergence toward globally optimal solutions is achieved under convex problem settings.
- The enhanced version of the ADMM algorithm embeds carbon tax signals directly into the iterative update of exchange prices. Unlike conventional methods that statically append a carbon price term to the cost function, our mechanism dynamically adjusts power exchange tariffs during each iteration, based on both the upstream grid's time-varying carbon intensity and local gas turbine emissions. This feedback-driven design ensures that carbon considerations actively influence the optimization trajectory of all agents. As a result, the framework steers microgrid and DNO scheduling decisions toward low-carbon outcomes in real time, rather than simply penalizing emissions after decisions are made.
- A robust optimization framework is embedded within the planning processes of all agents to safeguard day-ahead schedules against deviations in renewable generation and load demand. This ensures that real-time feasibility is preserved even under uncertain operating conditions. Unlike existing works that overlook the impact of such uncertainty and leave agents exposed to reliance on expensive spot market purchases, our approach explicitly minimizes this reliance. The result is a substantial reduction in operational costs and enhanced resilience of market participation, demonstrating the capacity of the proposed method to deliver both economic and environmental benefits under realistic uncertainty conditions.

2. Model description

This paper presents a comprehensive optimization framework for the settlement of distribution-level day-ahead electricity markets, addressing three critical objectives: (a) preserving the information security of all participating agents, (b) maximizing the potential of residential and industrial microgrids to reduce carbon emissions, and (c) ensuring the real-time feasibility of all confirmed power exchange contracts from the day-ahead market.

In this study, the DNO clears the distribution-level day-ahead market by coordinating residential and industrial microgrids subject to network constraints. The transmission-level market organized by the ISO is not modeled; instead, upstream electricity price and carbon-intensity signals enter the DNO problem as exogenous time-varying parameters. This separation allows us to focus on the integration and coordination of flexible resources at the distribution level (storage systems, V2G technologies, flexible loads) using the proposed enhanced ADMM with dynamic carbon-tax signals and robust scheduling. The interface with the transmission system is represented by the net power exchange at the root bus, making the framework compatible with any ISO market formulation without requiring joint co-optimization.

The proposed framework, illustrated in Fig. 1, consists of two layers designed to coordinate decentralized residential and industrial microgrids with the DNO while addressing the specified objectives. In the upper layer, individual residential and industrial microgrids perform day-ahead planning to optimize costs and submit their preferred schedules for power exchange to the DNO, which acts as the distribution-level market organizer. These schedules, defined on an hourly basis over a 24-hour horizon, specify the intended power purchases or sales for each microgrid. In the lower layer, the DNO incorporates the received schedules into a network-constrained planning process, ensuring the feasibility of market commitments while aiming to minimize system costs. A robust optimization approach is employed for all agents (DNO and microgrids) to safeguard their day-ahead plans against real-time uncertainties caused by fluctuations in load demand and renewable generation from wind and solar resources.

To achieve distributed optimization, an enhanced version of the ADMM algorithm is developed. This algorithm enables efficient coordination between the upper and lower layers with minimal information exchange. Only coupling variables, representing power exchange between microgrids and the distribution system, are shared, ensuring the confidentiality of internal data for each agent. The iterative nature of the algorithm allows microgrid operators and the DNO to dynamically update their respective plans based on exchanged coupling variables and the plans of counterpart agents. A key feature of the proposed ADMM algorithm is the integration of a dynamic pricing mechanism, which updates the price of power exchanges in each iteration based on the discrepancy between coupling variables and the imposition of a carbon tax on power sourced from the upstream network. This mechanism ensures that the planning of all agents aligns with environmental objectives, promoting a reduction in carbon emissions.

It is important to emphasize that in the proposed two-layer framework, each agent, whether a residential or industrial microgrid, solves its own local optimization problem independently, based on its internal objectives, constraints, and operational models. These local models are neither shared with the DNO nor centrally coordinated. The DNO, functioning as the local market facilitator, solves its own network-constrained optimization problem using only the power exchange plans submitted by the microgrids. This structure fully preserves the decentralized nature of real-life electricity markets, where market participants autonomously determine their offers or bids without disclosing their internal data. The ADMM serves solely as a coordination mechanism, enabling minimal information exchange by iteratively updating coupling variables and price signals between agents and the DNO. No central entity runs the entire model; instead, the coordination emerges

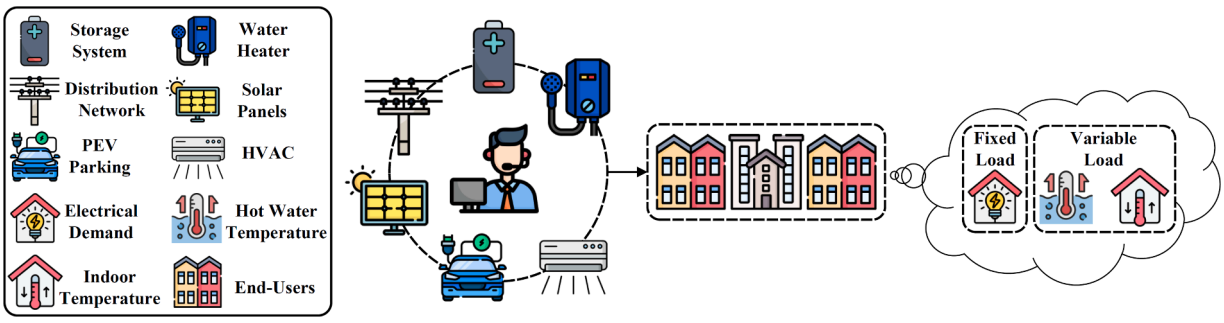

Fig. 2. Internal structure of the residential microgrids under investigation.

through the distributed solution process, which accurately reflects how real-world decentralized markets operate.

3. Mathematical formulation

The formulation presented in this section represents the proposed two-layer model in the form of a MILP problem. In the upper layer, the model independently formulates residential and industrial microgrids, considering their specific components and individual objective functions. Meanwhile, the lower layer formulates the distribution network, considering its topology, components, objective function, and linear AC power flow framework. After independently formulating the two proposed layers, subsection 3.3 presents a robust optimization technique to handle uncertainties associated with various agents within each layer, while section 3.4 describes the mechanism for linking them through a novel enhanced ADMM algorithm.

3.1. Layer 1

3 1 1. . Residential microgrids

The residential microgrids analyzed in this study are designed to supply both electrical and thermal demands for subscribers within their service area, as shown in Fig. 2. These microgrids are capable of bi-directional power exchange with the distribution network and are equipped with solar panels, electrical storage systems, electric water heaters, heating, ventilation, and air conditioning (HVAC) systems, and parking lots for PEVs capable of V2G services. The total load of each residential microgrid consists of two components: a fixed part and a variable part. The variable component depends on the operational settings of HVAC and electric water heater systems, which are adjusted based on the temperatures for indoor spaces and hot water.

The objective function of the residential microgrids, as presented in (a1), aims to minimize the total operational costs in the day-ahead electricity market. This function includes four key cost components: (1) costs associated with grid power exchanges, (2) costs for charging and discharging energy storage systems, (3) costs related to procuring V2G services, and (4) penalties for deviations from the subscriber welfare index. It should be stated that the electricity tariff ($\lambda_{r,t}^{Exch}$) for power exchange with the grid is dynamic and will be determined using the proposed enhanced ADMM algorithm, which is elaborated in Subsection 3.4. The welfare index penalty in the objective function explicitly quantifies the trade-off between minimizing operational costs and maintaining residential comfort, ensuring that flexible load adjustments do not significantly compromise user-defined temperature preferences within acceptable comfort limits. This index, defined in (a2), quantifies the deviation of optimized indoor and hot water temperatures from their desired setpoints. A welfare index of 100 indicates a perfect match, while deviations reduce the index proportionally. To ensure acceptable comfort levels, the maximum allowable deviation is limited to $\varepsilon = 0.09$ as specified in (a3). Equation (a4) models the power balance for each residential microgrid by incorporating all components, loads, and power exchanges with the grid.

$$Cost_r^{MG} = \sum_t \left(\lambda_{r,t}^{Exch} P_{r,t}^{Exch}\right)\Delta t + \sum_t \left[\lambda_r^{Storage}\left(P_{r,t}^{Charge} + P_{r,t}^{Discharge}\right)\right]\Delta t + \sum_t \left(\lambda_r^{V2G} P_{r,t}^{V2G}\right)\Delta t + \sum_t \left(\lambda_r^{Dev}\left|WI_{r,t}^{MG.Desire} - WI_{r,t}^{MG}\right|\right) \tag{a1}$$

$$WI_r^{MG} = \left(1 - \delta^{Water}\left|T_{r,t}^{Water.Desire} - T_{r,t}^{Water}\right| - \delta^{Air}\left|T_{r,t}^{Air.Desire} - T_{r,t}^{Air}\right|\right) \times 100 \tag{a2}$$

$$\begin{cases} (1-\varepsilon)T_{r,t}^{Water.Desire} \le T_{r,t}^{Water} \le (1+\varepsilon)T_{r,t}^{Water.Desire} \\ (1-\varepsilon)T_{r,t}^{Air.Desire} \le T_{r,t}^{Air} \le (1+\varepsilon)T_{r,t}^{Air.Desire} \end{cases} \tag{a3}$$

$$P_{r,t}^{Exch} = P_{r,t}^{Fixed} + P_{r,t}^{Variable} - P_{r,t}^{Solar} + P_{r,t}^{Charge} - P_{r,t}^{Discharge} + \sum_{v\in\Omega_r^v}\left(P_{v,t}^{G2V} - P_{v,t}^{V2G}\right) \tag{a4}$$

The mathematical representation of the solar panel system integrated with battery storage within residential microgrids is outlined in (a5)-(a11). Equation (a5) calculates the electricity generation of solar panels as a function of solar irradiance $Irradiance_t$, rated irradiance $Irradiance^{Max}$, panel efficiency ϖ^{Solar}, and the panel's capacity $P_r^{Solar.Capacity}$. Constraints (a6) and (a7) define the operational boundaries for battery charging and discharging processes. These constraints ensure that the power remains within the maximum allowable limits, controlled by binary variables $u_{r,t}^{Charge}$ and $u_{r,t}^{Discharge}$ that indicate whether charging or discharging is active. Constraint (a8) enforces operational exclusivity by prohibiting simultaneous charging and discharging, requiring the sum of the binary variables to be no greater than one. The state of charge (SoC) of the battery is updated in (a9), which considers the energy stored or released during each time step Δt, incorporating charging and discharging efficiencies. The final SoC value is specified in (a10) to maintain energy consistency across the planning horizon.

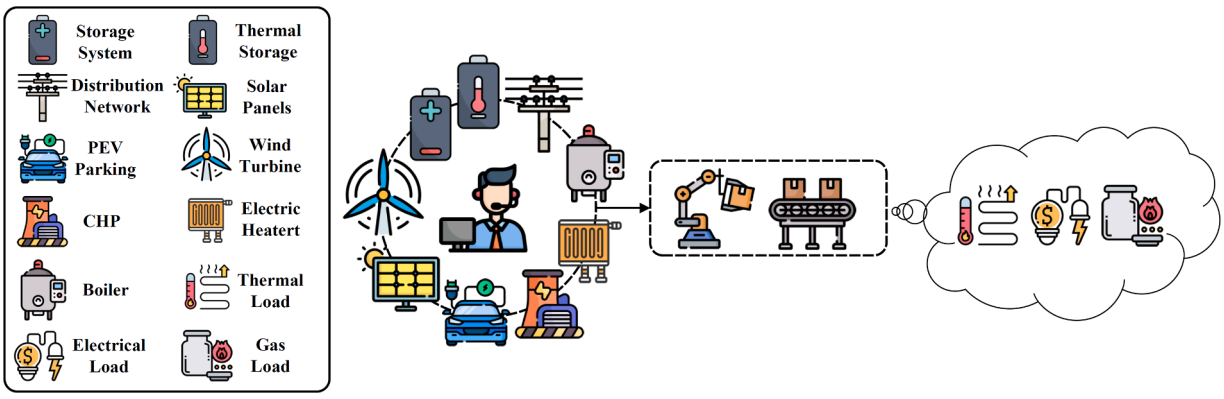

Fig. 3. Internal structure of the industrial microgrids under investigation.

Finally, (a11) ensures that the battery's energy levels remain within the predefined upper and lower bounds throughout its operation.

$$P_{r,t}^{Solar} = \varpi^{Solar} \frac{Irradiance_t}{Irradiance^{Max}} P_r^{Solar,Capacity} \tag{a5}$$

$$0 \le P_{r,t}^{Charge} \le P_r^{Charge,Max} u_{r,t}^{Charge} \tag{a6}$$

$$0 \le P_{r,t}^{Discharge} \le P_r^{Discharge,Max} u_{r,t}^{Discharge} \tag{a7}$$

$$u_{r,t}^{Charge} + u_{r,t}^{Discharge} \le 1 \tag{a8}$$

$$E_{r,t}^{Storage} = E_r^{Storage,0} + \sum_{k \le t} \left(P_{r,k}^{Charge} - P_{r,k}^{Discharge} \right) \Delta t \tag{a9}$$

$$E_{r,t=T}^{Storage} = E_r^{Storage,0} \tag{a10}$$

$$E_r^{Storage,Min} \le E_{r,t}^{Storage} \le E_r^{Storage,Max} \tag{a11}$$

The EWH systems within residential microgrids are formulated in (a12)-(a17) (Mansouri et al., 2024). Equation (a12) models the water temperature at time t, which is influenced by the previous water temperature $T_{r,t-1}^{Water}$, the power supplied to the EWH $P_{r,t}^{Heater}$, energy losses $E_{r,t}^{Heater}$, and parasitic thermal losses $E_{r,t}^{Heater,Loss}$. Here, ϑ represents the thermal constant of water, and $W_{r,t}^{Demand}$ denotes the water demand. The water temperature is initialized to a predefined value $T_r^{Water,0}$ as specified in (a13). Constraint (a14) ensures the water temperature remains within an acceptable range throughout the scheduling horizon. Equation (a15) calculates the energy required to heat water from its initial cold state $T_r^{Water,Cold}$ to the desired temperature $T_{r,t}^{Water}$. Parasitic thermal losses, modeled in (a16), considering heat transfer between the water in the tank and its surroundings. These losses depend on the temperature difference between the water ($T_{r,t}^{Water}$) and the ambient environment ($T_t^{Outside}$), the insulation properties of the tank (Δl), and the tank's heat transfer coefficient (κ). The total heat loss is further scaled by the tank's surface area (S_r^{Heater}). Constraint (a17) imposes an upper limit on the power input to the EWH.

$$T_{r,t}^{Water} = \frac{P_{r,t}^{Heater} \Delta t - E_{r,t}^{Heater} - E_{r,t}^{Heater,Loss}}{W_{r,t}^{Demand} \vartheta} + T_{r,t-1}^{Water} \tag{a12}$$

$$T_{r,t=0}^{Water} = T_r^{Water,0} \tag{a13}$$

$$T_r^{Water,Min} \le T_{r,t}^{Water} \le T_{r,t}^{Water,Max} \tag{a14}$$

$$E_{r,t}^{Heater} = W_{r,t}^{Demand} \vartheta \left(T_{r,t}^{Water} - T_r^{Water,Cold} \right) \tag{a15}$$

$$E_{r,t}^{Heater,Loss} = \frac{T_{r,t}^{Water} - T_t^{Outside}}{\frac{\Delta l}{\varphi} + \frac{1}{\kappa}} S_r^{Heater} \Delta t \tag{a16}$$

$$0 \le P_{r,t}^{Heater} \le P_r^{Heater,Max} \tag{a17}$$

The mathematical formulation of HVAC systems operating within residential microgrids is detailed in (a18)-(a22) (Mansouri et al., 2024). Equation (a18) models the indoor temperature variation $T_{r,t}^{Air}$ at time t as a function of the preceding indoor temperature, the external temperature $T_t^{Outside}$, and the system's power consumption $P_{r,t}^{Conditioner}$. Parameter ξ characterizes the thermal conductance of the building's structure, indicating how external conditions influence the indoor environment. The term $\varpi^{Conditioner}$ reflects the HVAC system's efficiency in modifying the indoor temperature per unit of power over a discrete time interval Δt. Constraint (a19) initializes the indoor temperature $T_{r,t=0}^{Air}$ to a predefined baseline value $T_r^{Air,0}$ to provide a reference for the simulation. Constraint (a20) establishes the permissible temperature range for indoor spaces over the scheduling horizon, with $T_r^{Air,Min}$ and $T_r^{Air,Max}$ denoting the minimum and maximum allowable limits. Constraint (a21) restricts the power consumption of the HVAC system to remain within operational bounds, ranging from zero to the maximum rated power $P_r^{Conditioner,Max}$. Lastly, (a22) introduces $P_{r,t}^{Variable}$ as the sum of the power consumed by the HVAC system and the EWH.

$$T_{r,t}^{Air} = (1 - \xi) T_{r,t-1}^{Air} + T_t^{Outside} \xi + \varpi^{Conditioner} P_{r,t}^{Conditioner} \Delta t \tag{a18}$$

$$T_{r,t=0}^{Air} = T_r^{Air,0} \tag{a19}$$

$$T_r^{Air,Min} \le T_{r,t}^{Air} \le T_r^{Air,Max} \tag{a20}$$

$$0 \le P_{r,t}^{Conditioner} \le P_r^{Conditioner,Max} \tag{a21}$$

$$P_{r,t}^{Variable} = P_{r,t}^{Conditioner} + P_{r,t}^{Heater} \tag{a22}$$

The residential microgrids incorporate parking lots designated for PEVs, capable of delivering V2G services (Mansouri et al., 2023). These services rely on the strategic scheduling of charging and discharging activities involving PEV batteries, constrained by the entry and exit times of the vehicles and their respective energy levels. Constraints (a23) to (a25) define the operational limits for charging and discharging, with binary indicators $u_{v,t}^{G2V}$ and $u_{v,t}^{V2G}$ controlling these states. The energy stored in the batteries is calculated in (a26), which accounts for energy transfers during both charging and discharging, taking into account efficiency losses. Additionally, (27) and (28) specify the battery energy levels at arrival and departure times, while (29) establishes the range of allowable energy levels at intermediate time intervals.

$$0 \le P_{v,t}^{G2V} \le P_v^{G2V,Max} u_{v,t}^{G2V} \tag{a23}$$

$$0 \le P_{v,t}^{V2G} \le P_{v}^{V2G,Max} u_{v,t}^{V2G} \tag{a24}$$

$$u_{v,t}^{G2V} + u_{v,t}^{V2G} \le 1 \tag{a25}$$

$$E_{v,t}^{PEV} = E_{v,t=Ar_v}^{PEV} + \sum_{k \le t} \left(P_{v,t}^{G2V} - P_{v,t}^{V2G} \right) \Delta t \tag{a26}$$

$$E_{v,t=Ar_v}^{PEV} = \alpha^{Ar} E_{v}^{PEV,Max} \tag{a27}$$

$$Cost_i^{MG} = \sum_t \left[\lambda_{i,t}^{Exch} \begin{pmatrix} P_{i,t}^{Grid \to Demand} + P_{i,t}^{Grid \to Heater} \\ + P_{i,t}^{Grid \to Storage} \end{pmatrix} \right] \Delta t + \sum_t \left[\lambda_{i,t}^{Gas} \begin{pmatrix} G_{i,t}^{Grid \to Demand} + G_{i,t}^{Grid \to CHP} \\ + G_{i,t}^{Grid \to Boiler} \end{pmatrix} \right] \Delta t$$
$$+ \sum_t \left[\lambda_i^{Storage} \begin{pmatrix} P_{i,t}^{Charge} + P_{i,t}^{Discharge} \\ + H_{i,t}^{Charge} + H_{i,t}^{Discharge} \end{pmatrix} \right] \Delta t + \sum_t \left(\lambda_i^{V2G} P_{i,t}^{V2G} \right) \Delta t + \sum_t \left(\lambda_i^{Dev} \Delta M6_{i,t} \right) \tag{b1}$$

$$E_{v,t=Dp_v}^{PEV} = \alpha^{DP} E_{v}^{PEV,Max} \tag{a28}$$

$$E_{v}^{PEV,Min} \le E_{v,t}^{PEV} \le E_{v}^{PEV,Max} \tag{a29}$$

3.1.2. Industrial Microgrids

Fig. 3 illustrates the internal structure of the industrial microgrids under analysis. These microgrids integrate diverse energy sources, such as wind turbines, solar panels, combined heat and power (CHP) units, electric heaters, and boilers, as well as electrical and thermal storage systems and V2G-enabled PEV parking lots. Their primary role is to support various production activities, culminating in the creation of multiple goods. Industrial microgrids maintain connections with both electricity and gas networks to meet their energy requirements, ensuring a steady supply of electrical, thermal, and gas energy. Electricity is sourced from the distribution grid and on-site generators, including CHP systems, wind turbines and solar panels, while gas is procured directly from the network. Heat generation is also driven by the CHP units, electric heaters, and boilers. As represented in Fig. 3, the manufacturing process produces six unique materials. Materials 1 to 5 can either be utilized in subsequent production phases or stored for future use. The sixth material, the final product, has two potential destinations: storage in the warehouse or direct sale in the market.

The objective function described in (b1) aims to minimize the day-ahead scheduling costs associated with industrial microgrids. It comprises five cost components: the electricity procurement cost from the grid, the gas procurement cost, the operational costs of electrical and thermal storage systems, the fee paid to PEV users for providing V2G, and penalties incurred for deviations from the scheduled production of the end material. The deviation is quantified by comparing the preferred schedule with the finalized schedule for the production rate of the end material, as specified in (b2).

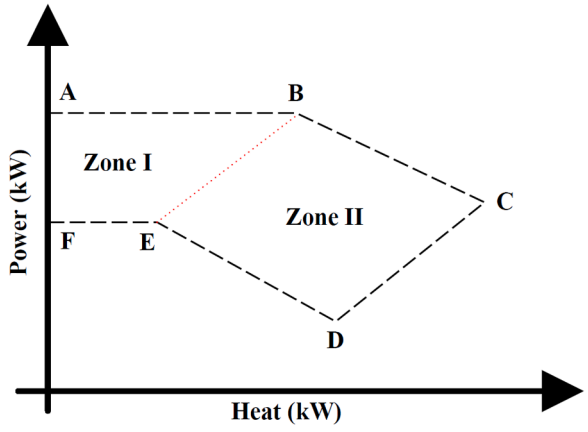

Fig. 4. Operational regions of the CHP unit.

$$\begin{cases} \Delta M6_{i,t} \ge M6_{i,t}^{P6,Desire} - M6_{i,t}^{P6,Ch} \\ \Delta M6_{i,t} \ge M6_{i,t}^{P6,Ch} - M6_{i,t}^{P6,Desire} \end{cases} \tag{b2}$$

The operational behavior of CHP units within industrial microgrids, as described by (b3)-(b12), is divided into two distinct operational zones illustrated in Fig. 4 (Alomoush, 2020). Constraint (b3) determines the active zone of the CHP unit, with the binary variable $u_{i,t}^{I}$ set to 1 for zone I and $u_{i,t}^{II}$ set to 1 for zone II. The binary variable $u_{i,t}^{CHP}$ dictates the unit's operational state, indicating whether it is switched on or off. Constraints (b4) and (b5) define the maximum allowable electrical (P_i^A) and thermal (H_i^C) outputs, ensuring both values remain zero when the unit is inactive. Further, constraints (b6)-(b11) outline the feasible output ranges for the electrical and thermal energy produced in each operational zone, with boundaries governed by the activation state of the respective binary variables. These constraints ensure the CHP operates within predefined physical and safety limits, maintaining efficiency and reliability. Eventually, (b12) computes the gas consumption of the CHP, taking into account both its electrical and thermal output levels.

$$u_{i,t}^{I} + u_{i,t}^{II} = u_{i,t}^{CHP} \tag{b3}$$

$$0 \le P_{i,t}^{CHP} \le P_i^A u_{i,t}^{CHP} \tag{b4}$$

$$0 \le H_{i,t}^{CHP} \le H_i^C u_{i,t}^{CHP} \tag{b5}$$

$$0 \le H_{i,t}^{CHP} - H_i^E \le \left(1 - u_{i,t}^{I}\right)\left(H_i^C - H_i^E\right) \tag{b6}$$

$$0 \le P_{i,t}^{CHP} - P_i^E \ge \left(u_{i,t}^{I} - 1\right) P_i^E \tag{b7}$$

$$0 \le H_{i,t}^{CHP} - H_i^E \ge \left(u_{i,t}^{II} - 1\right) H_i^E \tag{b8}$$

$$P_{i,t}^{CHP} - P_i^D - \frac{P_i^D - P_i^E}{H_i^D - H_i^E}\left(H_{i,t}^{CHP} - H_i^D\right) \ge \left(u_{i,t}^{II} - 1\right)\left(P_i^D - \frac{\left(P_i^D - P_i^E\right)\left(H_i^D\right)}{H_i^D - H_i^E}\right) \tag{b9}$$

$$P_{i,t}^{CHP} - P_i^B - \frac{P_i^B - P_i^C}{H_i^B - H_i^C}\left(H_{i,t}^{CHP} - H_i^C\right) \le \left(1 - u_{x,t}^{II}\right) \left(P_i^A - P_i^B - \frac{\left(P_i^B - P_i^C\right)\left(H_i^C - H_i^B\right)}{H_i^B - H_i^C}\right) \tag{b10}$$

$$P_{i,t}^{CHP} - P_i^C - \frac{P_i^C - P_i^D}{H_i^C - H_i^D}\left(H_{i,t}^{CHP} - H_i^C\right) \geq \left(u_{i,t}^{II} - 1\right)P_i^C \tag{b11}$$

$$G_{i,t}^{CHP} = a_i P_{i,t}^{CHP} + b_i H_{i,t}^{CHP} + c_i\left(P_{i,t}^{CHP}\right)^2 + d_i\left(H_{i,t}^{CHP}\right)^2 + e_i P_{i,t}^{CHP} H_{i,t}^{CHP} + f_i u_{i,t}^{CHP} \tag{b12}$$

The wind turbine's power generation is described by (b13), expressed as a piecewise function of wind speed. The model identifies three distinct operational stages: (1) no power is generated when the wind speed (v_t) is below the cut-in threshold (v_i^{CI}), (2) the power output increases linearly as the wind speed ranges between the cut-in speed and the rated wind speed (v_i^R), and (3) the turbine achieves its maximum power output ($P_i^{Wind,Capacity}$) when the wind speed lies between the rated wind speed and the cut-out threshold (v_i^{CO}). The model for PV panels in industrial microgrids is derived from the framework established for residential microgrids and is thus not repeated here.

$$P_{i,t}^{Wind} = \begin{cases} 0, v_t < v_i^{CI} or v_t \geq v_i^{CO} \\ P_i^{Wind,Capacity}\dfrac{v_t - v_i^R}{v_i^{CI} - v_i^R}, v_i^{CI} \leq v_t < v_i^R \\ P_i^{Wind,Capacity}, v_i^R \leq v_t < v_i^{CO} \end{cases} \tag{b13}$$

The heat production of the boiler is modeled in (b14), where the generated heat $H_{i,t}^{Boiler}$ depends on the gas consumption $G_{i,t}^{Boiler}$ and the associated efficiency factor $\alpha_{gas\to heat}^{Boiler}$. The maximum heat output is constrained in (b15), which limits it to the boiler's rated capacity. Similarly, (b16) defines the heat generation of the electric heater as a function of its electricity consumption $P_{i,t}^{Heater}$ and efficiency factor $\alpha_{elec\to heat}^{Heater}$. To ensure operational limits, (b17) imposes an upper bound on the electric heater's maximum heat output.

$$H_{i,t}^{Boiler} = \alpha_{gas\to heat}^{Boiler} G_{i,t}^{Boiler} \tag{b14}$$

$$H_{i,t}^{Boiler} \leq H_i^{Boiler,Max} \tag{b15}$$

$$H_{i,t}^{Heater} = \alpha_{elec\to heat}^{Heater} P_{i,t}^{Heater} \tag{b16}$$

$$H_{i,t}^{Heater} \leq H_i^{Heater,Max} \tag{b17}$$

The model for V2G-enabled parking lots and energy storage systems in industrial microgrids builds upon the framework previously developed for residential microgrids and is therefore not reiterated here. The flow of power, gas, and heat within the industrial microgrid is governed by the relationships defined in (b18)-(b22). These include the gas supplied to the CHP unit and boiler, detailed in (b18) and (b19), respectively. The electricity directed to the electric heater is captured in (b20), while (b21) and (b22) describe the inputs of electricity and heat to the battery and thermal energy storage systems.

$$G_{i,t}^{CHP} = G_{i,t}^{Grid\to CHP} \tag{b18}$$

$$G_{i,t}^{Boiler} = G_{i,t}^{Grid\to Boiler} \tag{b19}$$

$$P_{i,t}^{Heater} = P_{i,t}^{Grid\to Heater} + P_{i,t}^{ESS\to Heater} + P_{i,t}^{Solar\to Heater} + P_{i,t}^{Wind\to Heater} \tag{b20}$$

$$P_{i,t}^{Charge} = P_{i,t}^{Grid\to Storage} + P_{i,t}^{Solar\to Storage} + P_{i,t}^{Wind\to Storage} + P_{i,t}^{CHP\to Storage} \tag{b21}$$

$$H_{i,t}^{Charge} = H_{i,t}^{CHP\to Storage} + H_{i,t}^{Boiler\to Storage} + H_{i,t}^{Heater\to Storage} \tag{b22}$$

The output energy flows from various components within the industrial microgrid, including power, gas, and heat, are described by (b23)-(b30). Specifically, the power and thermal outputs of the CHP unit are defined in (b23) and (b24). The heat transfers from the boiler and the electric heater are represented by (b25) and (b26), respectively. The power output of solar panels and wind turbines is captured in (b27) and (b28), respectively. Finally, (b29) and (b30) outline the power and thermal outputs from the electrical and thermal energy storage systems.

$$P_{i,t}^{CHP} = P_{i,t}^{CHP\to Grid} + P_{i,t}^{CHP\to Storage} + P_{i,t}^{CHP\to Heater} + P_{i,t}^{CHP\to Demand} \tag{b23}$$

$$H_{i,t}^{CHP} = H_{i,t}^{CHP\to Storage} + H_{i,t}^{CHP\to Demand} \tag{b24}$$

$$H_{i,t}^{Boiler} = H_{i,t}^{Boiler\to Storage} + H_{i,t}^{Boiler\to Demand} \tag{b25}$$

$$H_{i,t}^{Heater} = H_{i,t}^{Heater\to Storage} + H_{i,t}^{Heater\to Demand} \tag{b26}$$

$$P_{i,t}^{Solar} = P_{i,t}^{Solar\to Grid} + P_{i,t}^{Solar\to Storage} + P_{i,t}^{Solar\to Hetaer} + P_{i,t}^{Solar\to Demand} \tag{b27}$$

$$P_{i,t}^{Wind} = P_{i,t}^{Wind\to Grid} + P_{i,t}^{Wind\to Storage} + P_{i,t}^{Wind\to Hetaer} + P_{i,t}^{Wind\to Demand} \tag{b28}$$

$$P_{i,t}^{Discharge} = P_{i,t}^{Storage\to Grid} + P_{i,t}^{Storage\to Heater} + P_{i,t}^{Storage\to Demand} \tag{b29}$$

$$H_{i,t}^{Discharge} = H_{i,t}^{Storage\to Demand} \tag{b30}$$

The processes required for producing materials 1 to 6 are outlined in (b31)-(b36) (Hui et al., 2023). These tasks include a parameter ($\chi^{(\cdot),(\cdot)}$) that translates the consumed energy into the corresponding material output. The production limits for each material are set by (b37), ensuring the operations remain within defined boundaries. Constraints (b38) and (b39) govern the flexibility of the final material production rate. Specifically, (b38) permits dynamic adjustments to the hourly production rate of the final material ($M_{i,t}^{P6}$) within specified limits, while (b39) ensures that the cumulative 24-hour production meets the daily target. This ensures the overall production commitments remain intact, even with short-term variations. The inventory dynamics for materials 1 to 6 are described in (b40)-(b45), taking into account previous stock levels as well as the ongoing import and export rates. Constraint (b46) establishes minimum and maximum storage capacities for warehouses. Lastly, (b47) defines the initial inventory levels for each warehouse at the beginning of the planning horizon, providing a reference point for effective inventory management.

$$M1_{i,t}^{P1,Ch} = \chi^{P,P1} P_{i,t}^{P1} + \chi^{G,P1} G_{i,t}^{P1} \tag{b31}$$

$$M2_{i,t}^{P2,Ch} = \chi^{P,P2} P_{i,t}^{P2} + \chi^{H,P2} H_{i,t}^{P2} + \chi^{G,P2} G_{i,t}^{P2} + \chi^{M1,P2} M1_{i,t}^{P2,Dis} \tag{b32}$$

$$M3_{i,t}^{P3,Ch} = \chi^{P,P3} P_{i,t}^{P3} + \chi^{G,P3} G_{i,t}^{P3} + \chi^{M4,P3} M4_{i,t}^{P3,Dis} \tag{b33}$$

$$M4_{i,t}^{P4,Ch} = \chi^{P,P4} P_{i,t}^{P4} + \chi^{M1,P4} M2_{i,t}^{P4,Dis} \tag{b34}$$

$$M5_{i,t}^{M5,Ch} = \chi^{P,P5} P_{i,t}^{P5} + \chi^{H,P5} H_{i,t}^{P5} + \chi^{M3,P5} M3_{i,t}^{P5,Dis} \tag{b35}$$

$$M6_{i,t}^{P6,Ch} = \chi^{P,P6} P_{i,t}^{P6} + \chi^{H,P6} H_{i,t}^{P6} + \chi^{M2,P6} M2_{i,t}^{P6,Dis} + \chi^{M3,P6} M3_{i,t}^{P6,Dis} + \chi^{M4,P6} M4_{i,t}^{P6,Dis} + \chi^{M5,P6} M5_{i,t}^{P6,Dis} \tag{b36}$$

$$M_i^{P1/P2/P3/P4/P5,Min} \leq M_{i,t}^{P1/P2/P3/P4/P5,Ch} \leq M_i^{P1/P2/P3/P4/P5,Max} \tag{b37}$$

$$M6_{i,t}^{P6,Min} \leq M6_{i,t}^{P6,Ch} \leq M6_{i,t}^{P6,Max} \tag{b38}$$

$$\sum_t M6_{i,t}^{P6,Ch} = \sum_t M6_{i,t}^{P6,Desire} \tag{b39}$$

$$S_{i,t}^{M1} = S_{i,t-1}^{M1} + M1_{i,t}^{P1,Ch} - M1_{i,t}^{P2,Dis} \tag{b40}$$

$$S_{i,t}^{M2} = S_{i,t-1}^{M2} + M2_{i,t}^{P2,Ch} - M2_{i,t}^{P4,Dis} - M2_{i,t}^{P6,Dis} \tag{b41}$$

$$S_{i,t}^{M3} = S_{i,t-1}^{M3} + M3_{i,t}^{P3,Ch} - M3_{i,t}^{P5,Dis} - M3_{i,t}^{P6,Dis} \tag{b42}$$

$$S_{i,t}^{M4} = S_{i,t-1}^{M4} + M4_{i,t}^{P4,Ch} - M4_{i,t}^{P3,Dis} - M4_{i,t}^{P6,Dis} \tag{b43}$$

$$S_{i,t}^{M5} = S_{i,t-1}^{M5} + M5_{i,t}^{P5,Ch} - M5_{i,t}^{P6,Dis} \tag{b44}$$

$$S_{i,t}^{M6} = S_{i,t-1}^{M6} + M6_{i,t}^{P6,Ch} \tag{b45}$$

$$S_{i}^{M1/M2/M3/M4/M5/M6,Min} \le S_{i,t}^{M1/M2/M3/M4/M5/M6} \le S_{i}^{M1/M2/M3/M4/M5/M6,Max} \tag{b46}$$

$$S_{i,t=0}^{M1/M2/M3/M4/M5/M6} = S_{i}^{M1/M2/M3/M4/M5/M6,0} \tag{b47}$$

The power, gas, and thermal loads necessary for performing various operations within the industrial microgrid are characterized in (b48)-(b50). These energy demands can be fulfilled either by internal microgrid resources or through external connections to electricity and gas networks, depending on system availability and operational requirements.

$$P_{i,t}^{CHP\to Demand} + P_{x,t}^{Storage\to Demand} + P_{i,t}^{Solar\to Demand} + P_{i,t}^{Wind\to Demand} + P_{i,t}^{Grid\to Demand} = P_{i,t}^{P1} + P_{i,t}^{P2} + P_{i,t}^{P3} + P_{i,t}^{P4} + P_{i,t}^{P5} + P_{i,t}^{P6} \tag{b48}$$

$$G_{i,t}^{Grid\to Demand} = G_{i,t}^{P1} + G_{i,t}^{P2} + G_{i,t}^{P3} \tag{b49}$$

$$H_{i,t}^{CHP\to Demand} + H_{i,t}^{Boiler\to Demand} + H_{i,t}^{Heater\to Demand} + H_{i,t}^{Storage\to Demand} = H_{i,t}^{P2} + H_{i,t}^{P5} + H_{i,t}^{P6} \tag{b50}$$

3.2. Layer 2

The second layer of the proposed concept represents the DNO, which carries out security-constrained day-ahead scheduling for its service area. This scheduling incorporates the demand profiles submitted by first-layer agents, including residential and industrial microgrids. In (c1), the DNO's objective function is formulated to minimize the total costs, including energy procurement and operational expenses, while deducting the revenue generated from selling power to the microgrids. The first component reflects the cost of power exchange with the upstream electricity network, the second and third components represent the operational expenses of gas turbines and storage systems, respectively, and the fourth and fifth components correspond to the costs of power exchange with residential and industrial microgrids, respectively.

$$Cost^{DNO} = \sum_{t}\left(\lambda_{t}^{Grid}P_{t}^{Grid}\right)\Delta t + \sum_{t}\sum_{g}\left(\lambda_{g}^{Turbine}P_{g,t}^{Turbine}\right)\Delta t + \sum_{t}\sum_{e}\left[\lambda_{e}^{Storage}\left(P_{e,t}^{Charge} + P_{e,t}^{Discharge}\right)\right]\Delta t - \sum_{r}\sum_{t}\left(\lambda_{r,t}^{Exch}P_{r,t}^{Exch}\right)\Delta t - \sum_{i}\sum_{t}\left(\begin{array}{l} P_{i,t}^{Grid\to Demand} + P_{i,t}^{Grid\to Heater} \\ +P_{i,t}^{Grid\to Storage} \end{array}\right)\Delta t \tag{c1}$$

The distribution network incorporates various components, including gas turbines, wind turbines, solar panels, and electrical energy storage systems. Gas turbines are described by (c2)-(c4), while the modeling of wind turbines, solar panels, and energy storage systems adheres to the standard formulations applied to these systems within microgrids.

$$P_{g,t}^{Turbine} = \alpha_{gas\to elec}^{Turbine}G_{g,t}^{Turbine} \tag{c2}$$

$$P_{g}^{Turbine,Min} \le P_{g,t}^{Turbine} \le P_{g}^{Turbine,Max} \tag{c3}$$

$$Q_{g}^{Turbine,Min} \le Q_{g,t}^{Turbine} \le Q_{g}^{Turbine,Max} \tag{c4}$$

The linear AC power flow model used by the DNO to manage its service area is formulated through (c5)-(c12) (Mansouri et al., 2023). In (c5), the active power flow $P_{l,t}^{Line}$ along a transmission line is calculated as a linear function of voltage magnitudes and the phase angle differences between interconnected buses, normalized by the system base power S^{Base}. Similarly, (c6) defines the reactive power flow $Q_{l,t}^{Line}$. Power losses along the line, represented in (c7), naturally involve quadratic terms due to the combination of active $\left(P_{l,t}^{Line}\right)^2$ and reactive $\left(Q_{l,t}^{Line}\right)^2$ power components. To handle this, we have applied a piecewise linearization technique to approximate these quadratic loss terms using segmented linear functions (Xie & Sun, 2022), ensuring full compatibility with the MILP structure required for the CPLEX solver. For safe network operation, (c8) enforces that the power flow does not exceed the line's thermal capacity S_{l}^{Line}. Voltage magnitude limits at each bus are imposed in (c9), while (c10) ensures phase angle differences remain within system stability limits. Finally, (c11) and (c12) maintain power balance by ensuring consistent active and reactive power flows across the distribution network's service area.

$$\frac{P_{l,t}^{Line}}{S^{Base}} = G_{l}\left(Vol_{n,t} - Vol_{m,t}\right) + B_{l}\left(\theta_{n,t} - \theta_{m,t}\right) \tag{c5}$$

$$\frac{Q_{l,t}^{Line}}{S^{Base}} = B_{l}\left(Vol_{n,t} - Vol_{m,t}\right) - G_{l}\left(\theta_{n,t} - \theta_{m,t}\right) \tag{c6}$$

$$P_{l,t}^{Loss} = \frac{R_{l}\left[\left(P_{l,t}^{Line}\right)^2 + \left(Q_{l,t}^{Line}\right)^2\right]}{\left(S^{Base}\right)^2} \tag{c7}$$

$$\left(P_{l,t}^{Line}\right)^2 + \left(Q_{l,t}^{Line}\right)^2 \le \left(S_{l}^{Line}\right)^2 \tag{c8}$$

$$Vol_{n}^{Min} \le Vol_{n,t} \le Vol_{n}^{Max} \tag{c9}$$

$$\theta_{n}^{Min} \le \theta_{n,t} \le \theta_{n}^{Max} \tag{c10}$$

$$P_t^{Grid}\big|_{i=1} + \sum_{g\in\Omega_n^g} P_{g,t}^{Turbine} + \sum_{s\in\Omega_n^s} P_{s,t}^{Solar} + \sum_{w\in\Omega_n^w} P_{w,t}^{Wind} = P_n^{Demand} + \sum_{r\in\Omega_n^r} P_{r,t}^{Exch} + \sum_{i\in\Omega_n^i}\left(P_{i,t}^{Grid\to Demand} + P_{i,t}^{Grid\to Heater} + P_{i,t}^{Grid\to Storage}\right) + \sum_{l\in\Omega_n^l}\left(\kappa_{n,l}^{Flow} P_{l,t}^{Line} + \frac{P_{l,t}^{Loss} S^{Base}}{2}\right) \tag{c11}$$

$$Q_t^{Grid}\big|_{i=1} + \sum_{g\in\Omega_n^g} Q_{g,t}^{Turbine} = Q_n^{Demand} + \sum_{l\in\Omega_n^l}\left(\kappa_{n,l}^{Flow} Q_{l,t}^{Line}\right) + \sum_{r\in\Omega_n^r}\left(\gamma_r P_{r,t}^{Exch}\right) + \sum_{i\in\Omega_n^i}\left[\gamma_i\left(P_{i,t}^{Grid\to Demand} + P_{i,t}^{Grid\to Heater} + P_{i,t}^{Grid\to Storage}\right)\right] \tag{c12}$$

3.3. Robust optimization modelling

The framework detailed in (d1)-(d10) provides a robust optimization methodology applicable to all agents across both the first and second layers, including residential and industrial microgrids and the DNO (Zhang et al., 2024). It enables reliable day-ahead scheduling by incorporating uncertainties in renewable energy generation and load demands. Constraint (d1) represents the uncertain renewable generation as the sum of its forecasted value $\widehat{P}_{s/w,t}^{Solar/Wind}$ and an error term $\alpha_{s/w,t}^{Solar/Wind}\overline{P}_{s/w,t}^{Solar/Wind}$, with the error term constrained by a maximum allowable deviation to maintain operational stability. Constraint (d2) restricts the error ratio to values between 0 and 1, thereby bounding deviations from the forecast within feasible limits. Constraint (d3) introduces an overall uncertainty budget $\psi_{s/w}^{Solar/Wind}$, ensuring that total deviations in renewable generation across all time periods remain within acceptable levels. Similarly, constraint (d4) models the uncertain load demand as the sum of its forecasted value $\widehat{P}_{i,t}^{Demand}$ and the associated error term $\alpha_{i,t}^{Demand}\overline{P}_{i,t}^{Demand}$, where the error is bounded by the maximum predefined deviation. Constraint (d5) ensures that the demand error ratio $\alpha_{i,t}^{Demand}$ remains within the range of 0 to 1, and constraint (d6) guarantees that the cumulative deviation in demand does not exceed the allocated uncertainty budget ψ_i^{Demand}.

The base power balance is presented in (d7), ensuring that the total power supply, including generation and imports, matches the total demand under normal operating conditions. To handle uncertainties, constraints (d8) and (d9) introduce dual variables $\Lambda_{s/w,t}^{Solar/Wind}$, $\Theta_{s/w}^{Solar/Wind}$, $\Lambda_{i,t}^{Demand}$, and Θ_i^{Demand}, which represent deviations in renewable energy generation and load demand. These dual variables adaptively adjust the system's constraints, providing enhanced flexibility and resilience against uncertainties. The power balance in (d10) is revised by incorporating dual variables, allowing the model to account for deviations in renewable generation and load demands.

$$P_{s/w,t}^{Solar/Wind} \in \left[\widehat{P}_{s/w,t}^{Solar/Wind} - \alpha_{s/w,t}^{Solar/Wind}\overline{P}_{s/w,t}^{Solar/Wind}, \widehat{P}_{s/w,t}^{Solar/Wind} + \alpha_{s/w,t}^{Solar/Wind}\overline{P}_{s/w,t}^{Solar/Wind}\right] \tag{d1}$$

$$0 \le \alpha_{s/w,t}^{Solar/Wind} \le 1, \Lambda_{s/w,t}^{Solar/Wind} \tag{d2}$$

$$\sum_t \alpha_{s/w,t}^{Solar/Wind} \le \psi_{s/w}^{Solar/Wind}, \Theta_{s/w}^{Solar/Wind} \tag{d3}$$

$$P_{i,t}^{Demand} \in \left[\widehat{P}_{i,t}^{Demand} - \alpha_{i,t}^{Demand}\overline{P}_{i,t}^{Demand}, \widehat{P}_{i,t}^{Demand} + \alpha_{i,t}^{Demand}\overline{P}_{i,t}^{Demand}\right] \tag{d4}$$

$$0 \le \alpha_{i,t}^{Demand} \le 1, \Lambda_{i,t}^{Demand} \tag{d5}$$

$$\sum_t \alpha_{i,t}^{Demand} \le \psi_i^{Demand}, \Theta_i^{Demand} \tag{d6}$$

$$P_t^{Controllable} + \sum_{s/w}\left(\widehat{P}_{s/w,t}^{Solar/Wind} - \alpha_{s/w,t}^{Solar/Wind}\overline{P}_{s/w,t}^{Solar/Wind}\right) = \sum_i\left(\widehat{P}_{i,t}^{Demand} + \alpha_{i,t}^{Demand}\overline{P}_{i,t}^{Demand}\right) \tag{d7}$$

$$\Lambda_{s/w,t}^{Solar/Wind} + \Theta_{s/w}^{Solar/Wind} \ge \overline{P}_{s/w,t}^{Solar/Wind} \tag{d8}$$

$$\Lambda_{i,t}^{Demand} + \Theta_i^{Demand} \ge \overline{P}_{i,t}^{Demand} \tag{d9}$$

$$P_t^{Controllable} + \left[\widehat{P}_{s/w,t}^{Solar/Wind} - \left(\psi_{s/w}^{Solar/Wind}\Theta_{s/w}^{Solar/Wind} + \Lambda_{s/w,t}^{Solar/Wind}\right)\right] = \left[\widehat{P}_{i,t}^{Demand} + \left(\psi_i^{Demand}\Theta_i^{Demand} + \Lambda_{i,t}^{Demand}\right)\right] \tag{d10}$$

3.5. An enhanced ADMM for linking first and second layers

The ADMM is a commonly utilized technique for addressing distributed optimization problems (Mansouri et al., 2025). It enables the division of a complex optimization task into smaller subproblems that can be solved independently, while ensuring coordination through iterative updates. In hierarchical optimization scenarios, such as those involving system operators and local agents like microgrids, ADMM facilitates efficient interaction, achieving globally optimal solutions in a decentralized manner. This study proposes an enhanced version of the ADMM algorithm aimed at improving convergence speed and adaptability. Unlike conventional ADMM, which relies on fixed parameters, the proposed approach dynamically modifies algorithmic parameters during each iteration. The information exchanged between microgrids and the DNO is limited to coupling variables related to power exchanges, ensuring that local scheduling data remains confidential. This preserves agent privacy while enhancing the efficiency of decentralized energy systems. Additionally, by incorporating carbon emissions into the dynamic price update process, the proposed ADMM incentivizes agents to align their internal schedules with the system's environmental objectives without directly interfering in their scheduling processes.

The mathematical model of the proposed version of the ADMM is defined in (e1)-(e10). Equations (e1) to (e3) modify the upper- and lower-layer objectives by introducing penalty terms $\| \widetilde{P}_{r,t}^{Exch} - P_{r,t}^{Exch}\|_2^2$ and $\| \widetilde{P}_{i,t}^{Grid\to Demand} - P_{i,t}^{Grid\to Demand}\|_2^2$ applied to the coupling variables representing power exchanges. These penalties are scaled by coefficients $\frac{\rho_r}{2}$ and $\frac{\rho_i}{2}$, which are updated dynamically at each iteration. The coupling variable $P_{r,t}^{Exch}/P_{i,t}^{Grid\to Demand}$ indicates the power exchange amount for the agent undergoing optimization, while $\widetilde{P}_{r,t}^{Exch}/\widetilde{P}_{i,t}^{Grid\to Demand}$ reflects the corresponding value previously determined by its counterparts. Constraint (e4) regulates power exchanges to maintain system consistency. It is important to emphasize that this procedure is not equivalent to simply adding a fixed carbon price term to the cost functions of the agents. In the proposed enhanced ADMM, carbon taxes are embedded in the iterative update of exchange tariffs (see Eqs. (e5)-(e7)). These taxes vary in real time with the upstream grid's carbon intensity and local gas turbine emissions, and are recalculated at each iteration. Consequently, the optimization process itself is continuously shaped by carbon signals, creating a dynamic feedback mechanism. This differs fundamentally from static carbon pricing, which only penalizes emissions once and does not adapt to system conditions or influence iterative coordination. Equation (e5) dynamically updates power exchange prices by considering both total carbon taxes and variations in the coupling variables. The total carbon taxes, determined by (e6), encompass the taxes on power purchased from the upstream network (μ_t^{Grid}) and those applied to power generated by gas turbines ($\mu_g^{Turbine}$). The formulation of total carbon taxes in (e6) accounts for both upstream electricity purchases, which have time-varying carbon intensities, and local gas turbines, which have fixed emission rates (Wu et al., 2025). This structure ensures

Table 1
Pseudocode for implementing the proposed version of ADMM.

1. Set the initial values; $\rightarrow \left\{ \begin{matrix} \widetilde{P}_{r,t}^{Exch}, \widetilde{P}_{i,t}^{Grid \rightarrow Demand}, \widetilde{P}_{i,t}^{Grid \rightarrow Heater} \\ \widetilde{P}_{i,t}^{Grid \rightarrow Storage}, \lambda_{r,t}^{Exch}, \lambda_{i,t}^{Exch}, \rho_r, \rho_i \end{matrix} \right\}$2. **While** $\left(R^{Primal} + R^{Dual} > \varepsilon\right)$, **do**:3. **For** residential microgrid ***r*, do**:4. Solve residential microgrids optimization problem **(e1)** to find optimal solution;5. Record optimal solution for residential microgrid ***r***;
$\rightarrow \widetilde{P}_{r,t}^{Exch} = P_{r,t}^{Exch}$
6. **End**7. **For** Industrial microgrid ***i*, do**:8. Solve industrial microgrids optimization problem **(e2)** to find optimal solution;9. Record optimal solution for residential microgrid ***i***;
$\rightarrow \widetilde{P}_{i,t}^{Grid \rightarrow Demand} = P_{i,t}^{Grid \rightarrow Demand}$
10. **End**11. Solve the DNO optimization problem **(e3)** to find optimal solution;12. Update power exchange price based on differences between optimal solution of upper-level and lower-level **(e5)**;
13. **For** hour ***t*, do**:14. Calculate carbon taxes based on optimal solutions of lower-level at hour ***t*** **(e6)**; $\rightarrow \mu_t$
15. **End**16. Update power exchange price dynamically using carbon taxes **(e7)**;
17. Calculate primal **(e8)** and dual **(e9)** residuals; $\rightarrow R^{Primal}, R^{Dual}$18. Update penalty coefficient **(e10)**;19. **End**

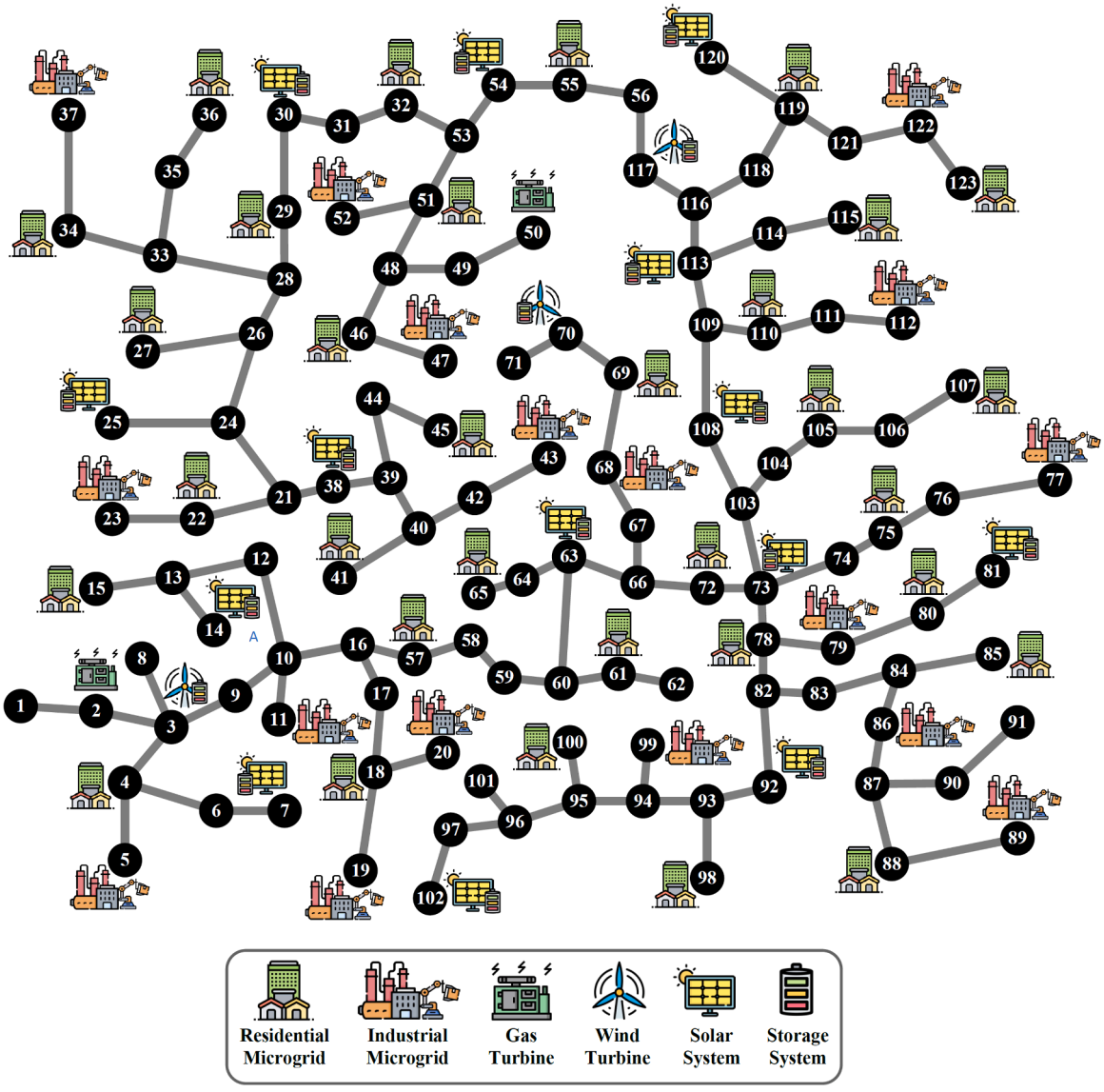

Fig. 5. Overview of the 123-bus electricity system under analysis.

that the environmental costs of all power sources are fully internalized in the agents' decision-making processes. The carbon taxes are then incorporated into the exchange prices, as calculated in (e5), through the adjustment defined in (e7). Equation (e8) calculates the primal residual, capturing differences in the coupling variables between iterations, while (e9) evaluates the dual residual, which measures changes in price updates. To enhance convergence speed, (e10) dynamically adjusts penalty coefficients based on the relative magnitude of the residuals. When the primal residual $R^{Primal}$is significantly larger than the dual residual R^{Dual},

the penalty coefficient is scaled up using the logarithmic term $\tau \log \frac{R^{Primal}}{R^{Dual}}$. Conversely, when R^{Dual} exceeds R^{Primal}, the penalty coefficient is scaled down using the logarithmic term $\tau \log \frac{R^{Dual}}{R^{Primal}}$. This adaptive adjustment mechanism enables the framework to respond dynamically to system behavior, leading to faster convergence compared to standard ADMM methods that use fixed parameters.

$$\mu_t = \mu_t^{Grid} + \frac{\sum_g \mu_g^{Turbine} P_{g,t}^{Turbine}}{\sum_g P_{g,t}^{Turbine} + \sum_s P_{s,t}^{Solar} + \sum_w P_{w,t}^{Wind}} \tag{e6}$$

$$\begin{aligned} Cost_r^{MG} = & \sum_t \left(\lambda_{r,t}^{Exch} P_{r,t}^{Exch}\right)\Delta t + \sum_t \left[\lambda_r^{Storage}\left(P_{r,t}^{Charge} + P_{r,t}^{Discharge}\right)\right]\Delta t + \sum_t \left(\lambda_r^{V2G} P_{r,t}^{V2G}\right)\Delta t \\ & + \sum_t \left(\lambda_r^{Dev}\left|WI_{r,t}^{MG,Desire} - WI_{r,t}^{MG}\right|\right) + \frac{\rho_r}{2}\| \widetilde{P}_{r,t}^{Exch} - P_{r,t}^{Exch} \|_2^2 \end{aligned} \tag{e1}$$

$$\begin{aligned} Cost_i^{MG} = & \sum_t \left[\lambda_{i,t}^{Exch}\begin{pmatrix} P_{i,t}^{Grid\to Demand} + P_{i,t}^{Grid\to Heater} \\ + P_{i,t}^{Grid\to Storage} \end{pmatrix}\right]\Delta t + \sum_t \left[\lambda_{i,t}^{Gas}\begin{pmatrix} G_{i,t}^{Grid\to Demand} + G_{i,t}^{Grid\to CHP} \\ + G_{i,t}^{Grid\to Boiler} \end{pmatrix}\right]\Delta t \\ & + \sum_t \left[\lambda_i^{Storage}\begin{pmatrix} P_{i,t}^{Charge} + P_{i,t}^{Discharge} \\ + H_{i,t}^{Charge} + H_{i,t}^{Discharge} \end{pmatrix}\right]\Delta t + \sum_t \left(\lambda_i^{V2G} P_{i,t}^{V2G}\right)\Delta t + \sum_t \left(\lambda_i^{Dev}\Delta M6_{i,t}\right) \\ & + \frac{\rho_i}{2}\| \widetilde{P}_{i,t}^{Grid\to Demand} + \widetilde{P}_{i,t}^{Grid\to Heater} + \widetilde{P}_{i,t}^{Grid\to Storage} - P_{i,t}^{Grid\to Demand} - P_{i,t}^{Grid\to Heater} - P_{i,t}^{Grid\to Storage} \|_2^2 \end{aligned} \tag{e2}$$

$$\begin{aligned} Cost^{DNO} = & \sum_t \left(\lambda_t^{Grid} P_t^{Grid}\right)\Delta t + \sum_t\sum_g \left(\lambda_g^{Turbine} P_{g,t}^{Turbine}\right)\Delta t + \sum_t\sum_e \left[\lambda_e^{Storage}\left(P_{e,t}^{Charge} + P_{e,t}^{Discharge}\right)\right]\Delta t \\ & - \sum_r\sum_t \left(\lambda_{r,t}^{Exch} P_{r,t}^{Exch}\right)\Delta t - \sum_i\sum_t \left[\lambda_{i,t}^{Exch}\begin{pmatrix} P_{i,t}^{Grid\to Demand} + P_{i,t}^{Grid\to Heater} \\ + P_{i,t}^{Grid\to Storage} \end{pmatrix}\right]\Delta t + \frac{\rho_r}{2}\| \widetilde{P}_{r,t}^{Exch} - P_{r,t}^{Exch} \|_2^2 \\ & + \frac{\rho_i}{2}\| \widetilde{P}_{i,t}^{Grid\to Demand} + \widetilde{P}_{i,t}^{Grid\to Heater} + \widetilde{P}_{i,t}^{Grid\to Storage} - P_{i,t}^{Grid\to Demand} - P_{i,t}^{Grid\to Heater} - P_{i,t}^{Grid\to Storage} \|_2^2 \end{aligned} \tag{e3}$$

$$\begin{cases} -P_r^{Exch,Max} \le P_{r,t}^{Exch} \le P_r^{Exch,Max} \\ P_i^{Exch,Max} \le P_{i,t}^{Grid\to Demand} + P_{i,t}^{Grid\to Heater} + P_{i,t}^{Grid\to Storage} \le P_i^{Exch,Max} \end{cases} \tag{e4}$$

$$\begin{cases} \lambda_{r,t}^{Exch,New} = \widetilde{\lambda}_{r,t}^{Exch,New} \dfrac{\mu_t}{\max(\mu_t)} \\ \lambda_{i,t}^{Exch,New} = \widetilde{\lambda}_{i,t}^{Exch,New} \dfrac{\mu_t}{\max(\mu_t)} \end{cases} \tag{e7}$$

$$\begin{cases} \lambda_{r,t}^{Exch,New} = \lambda_{r,t}^{Exch,Old} + \rho_r\left(P_{r,t}^{Exch} - \widetilde{P}_{r,t}^{Exch}\right) \\ \lambda_{i,t}^{Exch,New} = \lambda_{i,t}^{Exch,Old} + \rho_i\left(P_{i,t}^{Grid\to Demand} + P_{i,t}^{Grid\to Heater} + P_{i,t}^{Grid\to Storage} - \widetilde{P}_{i,t}^{Grid\to Demand} - \widetilde{P}_{i,t}^{Grid\to Heater} - \widetilde{P}_{i,t}^{Grid\to Storage}\right) \end{cases} \tag{e5}$$

Table 2
Scenarios under investigation.

Scenario	Dynamic Price Update Considering Carbon Taxes	Energy Storage Systems	V2G Services	Robust Scheduling	Coordination Mechanism
1	×	×	×	×	Proposed ADMM
2	✓	×	×	×	Proposed ADMM
3	✓	✓	×	×	Proposed ADMM
4	✓	✓	✓	×	Proposed ADMM
5	✓	✓	✓	✓	Proposed ADMM
6	✓	✓	✓	✓	Standard ADMM

$$R^{Primal} = \| \widetilde{P}_{r,t}^{Exch} - P_{r,t}^{Exch} \|_2 + \| \begin{matrix} \widetilde{P}_{i,t}^{Grid\to Demand} + \widetilde{P}_{i,t}^{Grid\to Heater} + \widetilde{P}_{i,t}^{Grid\to Storage} \\ -P_{i,t}^{Grid\to Demand} - P_{i,t}^{Grid\to Heater} - P_{i,t}^{Grid\to Storage} \end{matrix} \|_2 \quad \text{(e8)}$$

$$R^{Dual} = \| \lambda_{r,t}^{Exch,New} - \lambda_{r,t}^{Exch,Old} \|_2 + \| \lambda_{i,t}^{Exch,New} - \lambda_{i,t}^{Exch,Old} \|_2 \quad \text{(e9)}$$

$$\rho_{r/i} = \begin{cases} \rho_{r/i} + \tau \log \frac{R^{Primal}}{R^{Dual}}, R^{Primal} >> R^{Dual} \\ \rho_{r/i} - \tau \log \frac{R^{Dual}}{R^{Primal}}, R^{Dual} >> R^{Primal} \\ \rho_{r/i}, \text{Otherwise} \end{cases} \quad \text{(e10)}$$

The pseudocode provided in Table 1 has been designed to illustrate the step-by-step structure of the proposed enhanced ADMM algorithm. In each iteration, residential microgrids first solve their individual optimization problems independently, considering their local objectives and constraints. Once completed, industrial microgrids proceed with their own optimization based on their internal configurations. The DNO then solves its problem, incorporating the power exchange plans submitted by the microgrids and ensuring network feasibility. After solving these problems sequentially, the power exchange prices are dynamically updated by considering carbon tax signals and the differences between the exchanged power plans. Carbon taxes are recalculated in each iteration to influence pricing and encourage low-carbon scheduling. Primal and dual residuals are evaluated to monitor convergence, and the penalty coefficients are adaptively updated to accelerate the process. This iterative cycle continues until the sum of all primal and dual residuals falls below a predefined threshold ε, which is set to 0.001.

4. Simulation Results

The proposed two-layer model is tested on a 123-bus power

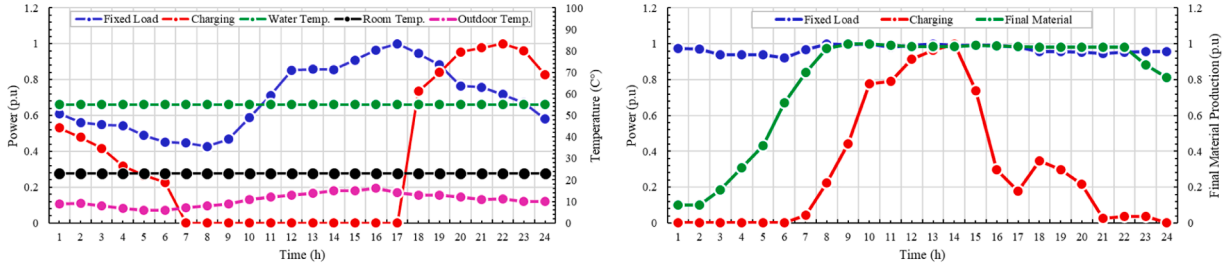

(a) Residential microgrids (b) Industrial microgrids

Fig. 6. Input parameters of residential and industrial microgrids.

Table 3
Details of microgrids and network components.

Residential Microgrids								
Connection Node			Solar System (kW)	Electric water Heater (kW)		Air Conditioner	No. of PEVs	Elec. Storage (kWh)
4, 15, 18, 22, 27, 29 32, 34, 36, 41, 45, 46			650	350		700	680	800
51, 55, 57, 61, 65, 69 72, 75, 78, 80, 85, 88			550	300		800	700	850
98, 100, 105, 107, 110, 115, 119, 123			700	250		750	600	900
Industrial Microgrids								
Connection Node	Solar System (kW)	Wind Turbine (kW)	Elec. Storage (kWh)	Ther. Storage (kWh)	No. of PEVs	CHP	Boiler	Electric Heater
5, 11, 19 20, 23, 37	800	1300	700	900	400	800	500	200
43, 47, 52 68, 77, 79	850	1000	800	1000	500	750	600	100
86, 89, 99 112, 122	900	1200	900	1100	450	650	500	150
Distribution Network Operator								
Wind Turbines			Solar Systems			Gas Turbines		
Connection Node	Capacity (kW)		Connection Node	Capacity (kW)		Connection Node	Capacity (kW)	
3, 70	1200		7, 14, 25, 30, 38 54, 63, 73	550		2	850	
117	1500		81, 92, 102, 108 113, 120	750		50	800	

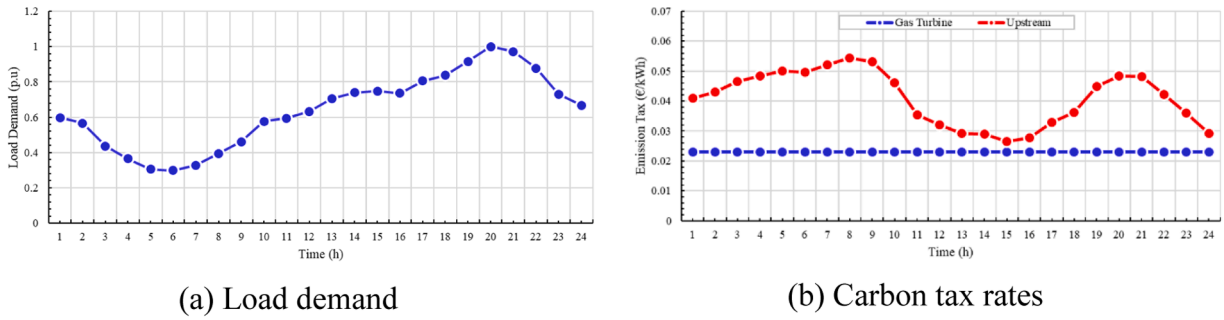

(a) Load demand (b) Carbon tax rates

Fig. 7. Input parameters of the DNO.

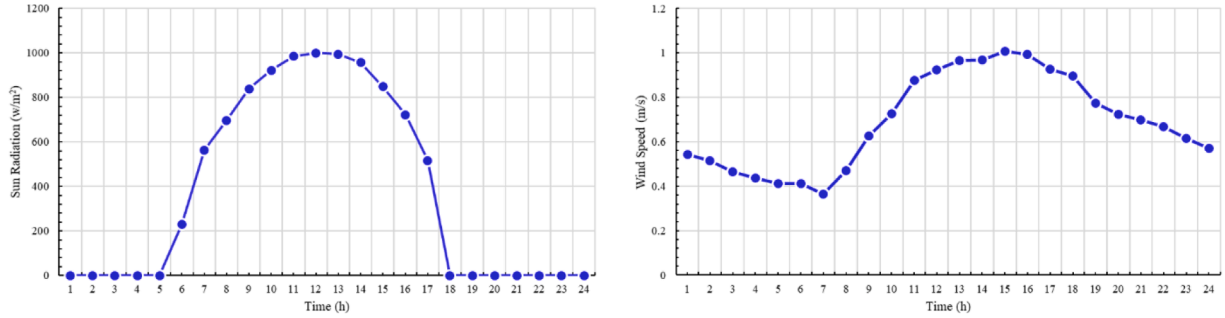

(a) Solar radiation (b) Wind speed

Fig. 8. Input parameters of renewable energy resources.

Table 4
Numerical outcomes derived from solving Scenario.1.

Agents	Day-Ahead Scheduling Costs (€)					Carbon Emissions (kg)
	Internal Technologies	Penalty for Deviating from Preferred Schedules	Exchange between DNO and Microgrids	Exchange between DNO and Upstream Network	Sum	
DNO	5041.21	-	-109746.34	103584.75	-1120.38	162574.96
Residential Microgrids	0	0	70884.37	-	70884.37	94405.98
Industrial Microgrids	0	0	38861.97	-	38861.97	56615.36
Total	5041.21	0	0	103584.75	108626	301690

Table 5
Numerical outcomes derived from solving Scenario 2.

Agents	Day-Ahead Scheduling Costs (€)					Carbon Emissions (kg)
	Internal Technologies	Penalty for Deviating from Preferred Schedules	Exchange between DNO and Microgrids	Exchange between DNO and Upstream Network	Sum	
DNO	5041.21	-	-114808.78	108330.63	-1436.94	139587.58
Residential Microgrids	0	158.65	72401.99	-	72560.64	88321.04
Industrial Microgrids	0	204.67	42406.79	-	42611.46	52225.69
Total	5041.21	363.32	0	108330.63	113735.2	280134.31

distribution network, depicted in Fig. 5. This network comprises 2 gas turbines, 3 wind units, 14 solar units, 17 electrical energy storage systems, and is coupled with 32 residential and 17 industrial microgrids. The model's performance is evaluated under six scenarios, detailed in Table 2, using the CPLEX solver in GAMS software. These scenarios aim to assess the model's capability to utilize microgrid flexible capacities for decarbonization, enhance the robustness of day-ahead schedules against real-time uncertainties, and improve the speed and accuracy of coordination among market agents. Fig. 6a and 6b illustrate the normalized input parameters for residential and industrial microgrids, respectively, which must be scaled using the capacities provided in Table 3. Table 3 further details the components of the microgrids and the distribution network. Fig. 7a shows the load demand curve of the distribution network, while Fig. 7b depicts the carbon tax rates applied to electricity procured from the upstream network and the gas turbines' output. Note that the carbon tax for gas turbine generation remains constant, whereas the tax for power purchased from the upstream network varies based on the proportion of renewable energy in the

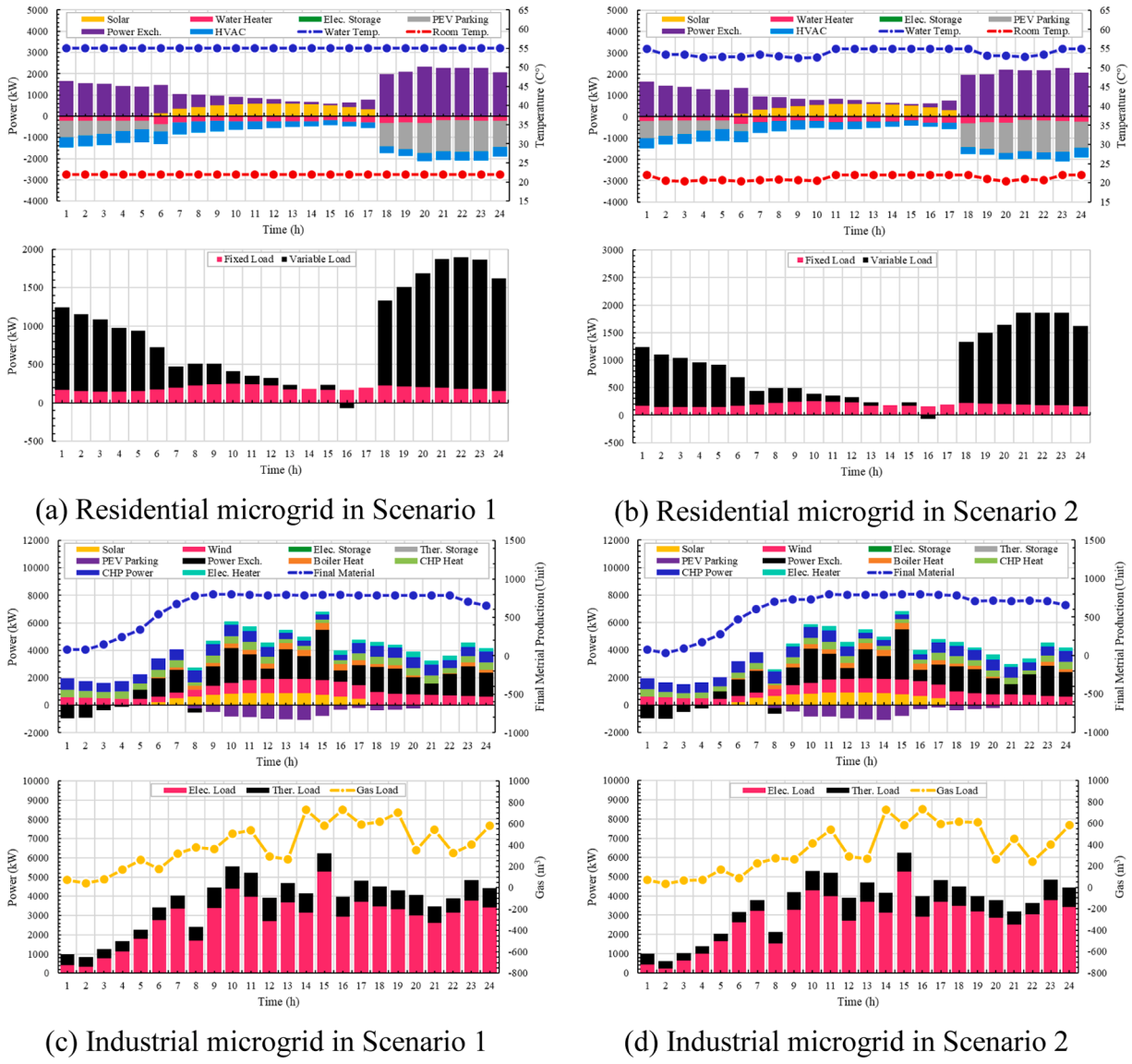

Fig. 9. Operational schedules obtained for microgrids in Scenarios 1 & 2.

network at different times. A higher renewable energy share results in lower tax coefficients, and vice versa. Finally, Figs. 8a and 8b present the input parameters associated with renewable energy units.

4 1. Results for scenarios 1 & 2

In Scenario 1, the proposed ADMM algorithm performs the dynamic price update process without incorporating carbon tax rates, while in Scenario 2, carbon tax rates are considered in the pricing mechanism. The results from these scenarios are summarized in Tables 4 and 5, respectively. Analysis reveals that including carbon tax rates in Scenario 2 leads to a 4.94 % increase in the total daily costs of the microgrids but achieves a 6.93 % reduction in total carbon emissions. Notably, in both scenarios, storage systems and V2G services remain inactive, leaving flexible load self-scheduling as the sole mechanism for operational adjustments.

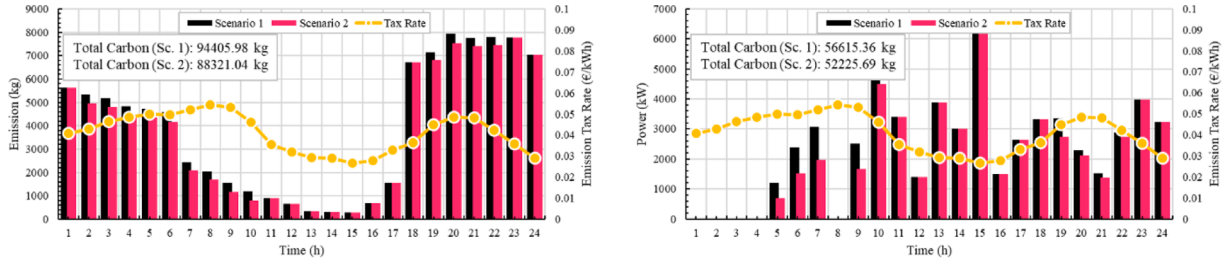

Fig. 10. Hourly carbon emissions of microgrids in Scenarios 1 & 2.

Table 6
Numerical outcomes derived from solving Scenario 3.

Agents	Day-Ahead Scheduling Costs (€)					Carbon Emissions (kg)
	Internal Technologies	Penalty for Deviating from Preferred Schedules	Exchange between DNO and Microgrids	Exchange between DNO and Upstream Network	Sum	
DNO	5981.33	-	-104196.35	96365.45	-1849.57	128232.69
Residential Microgrids	463.87	158.65	66355.19	-	66977.71	80943.14
Industrial Microgrids	512.37	204.67	37841.16	-	38558.2	48459.96
Total	6957.57	363.32	0	96365.45	103686.3	257635.79

Table 7
Numerical outcomes derived from solving Scenario 4.

Agents	Day-Ahead Scheduling Costs (€)					Carbon Emissions (kg)
	Internal Technologies	Penalty for Deviating from Preferred Schedules	Exchange between DNO and Microgrids	Exchange between DNO and Upstream Network	Sum	
DNO	5981.33	-	-95027.29	87036.22	-2009.74	116230.11
Residential Microgrids	795.33	158.65	61251.85	-	62205.83	74424.38
Industrial Microgrids	927.56	204.67	33775.44	-	34907.67	44745.7
Total	7704.22	363.32	0	87036.22	95103.76	235400.19

Fig. 9a-9d compare the operation plans for two microgrids, one residential and one industrial, connected to buses 36 and 122 of the distribution network, respectively, under Scenarios 1 and 2. The results show that adjusting the power exchange tariff to reflect carbon tax rates in Scenario 2 shifts the operational schedules of both residential and industrial microgrids. Specifically, both reduce their grid power purchases during peak price periods and shift these to off-peak periods. Since peak price periods correspond to high shares of fossil-fuel generation, reducing purchases during these times directly lowers carbon emissions. A detailed analysis indicates that the residential microgrid reduces hot water and room temperatures during peak periods, while the industrial microgrid shifts production rate of the final material to off-peak periods. This shift results in a permissible deviation in welfare indices: the residential microgrid experiences minor discomfort due to lower temperatures, and the industrial microgrid observes reduced production rate during peak price periods. The most significant welfare reduction occurs during these peak periods but remains within acceptable limits. This demonstrates that with minor welfare trade-offs, the microgrids substantially contribute to carbon emission reductions.

Fig. 10a and 10b illustrate the carbon emissions of residential and industrial microgrids under Scenarios 1 and 2. These Fig. show that in Scenario 2, carbon emissions during high carbon tax periods significantly decrease compared to Scenario 1, while emissions slightly increase during low carbon tax periods. Overall, Scenario 2 achieves a reduction of 6084.94 kg (6.44 %) in emissions for residential microgrids and 4389.67 kg (7.75 %) for industrial microgrids compared to Scenario 1. These findings confirm the effectiveness of integrating carbon tax rates into pricing mechanisms for promoting environmentally sustainable operation strategies.

4.2. Results for scenarios 3 & 4

In Scenarios 3 and 4, energy storage systems and V2G service provider technologies are activated, respectively, to evaluate the impact of the proposed model on leveraging their capacities for improving economic and environmental performance. The results from these scenarios are summarized in Tables 6 and 7. Numerical analysis reveals that activating storage systems in residential microgrids in Scenario 3 reduces operating costs by 7.69 % and carbon emissions by 8.35 % compared to Scenario 2, where these systems were inactive. This improvement is attributed to the enhanced flexibility of residential and industrial microgrid operators to modify their power exchange patterns with the network, enabled by the activation of electrical and thermal storage systems. Similarly, activating V2G technologies in Scenario 4 further enhances system flexibility, achieving an additional 7.12 % reduction in operating costs and a 8.05 % reduction in carbon emissions compared to Scenario 3.

Fig. 11a-11d illustrate the operational plans for residential and industrial microgrids connected to buses 36 and 122 under Scenarios 3 and 4. In Scenario 3, the activation of electrical storage in residential microgrids allows operators to purchase and store electricity during periods of lower carbon tax rates, reducing reliance on grid power during periods with higher carbon tax rates. Industrial microgrids adopt a similar strategy, leveraging their thermal storage systems to shift energy usage. Specifically, industrial operators increase the electric heater's operating point during low-carbon-tax periods to store heat, subsequently discharging stored heat during high-tax periods to reduce electricity consumption.

In Scenario 4, the activation of V2G technologies significantly enhances operational flexibility. Vehicle batteries are charged during periods with lower carbon tax rates and discharged during periods with higher rates, further reducing power imports during high-tax periods. This operational strategy is evident in the residential and industrial microgrid plans, which show marked shifts in power exchange patterns compared to Scenario 3. Fig. 12a and 12b present the hourly carbon emissions of residential and industrial microgrids under Scenarios 3 and 4. A comparison with Scenario 2, where storage systems and V2G technologies were inactive, highlights substantial reductions in emissions during periods with high carbon tax rates. Overall, the results from Scenarios 1 to 4 demonstrate that the proposed model effectively maximizes the flexible capacities of residential and industrial microgrids, aligning their operations with carbon emission reduction policies while achieving economic benefits.

4 3. Results for scenarios 5 & 6

Scenario 5 evaluates the performance of system agents, including the DNO and residential and industrial microgrids, in conducting day-ahead scheduling using a robust optimization technique. This approach explicitly incorporates uncertainties in load demand and wind and solar power generation. The results, summarized in Table 8, indicate that adopting the robust technique leads to increased day-ahead scheduling

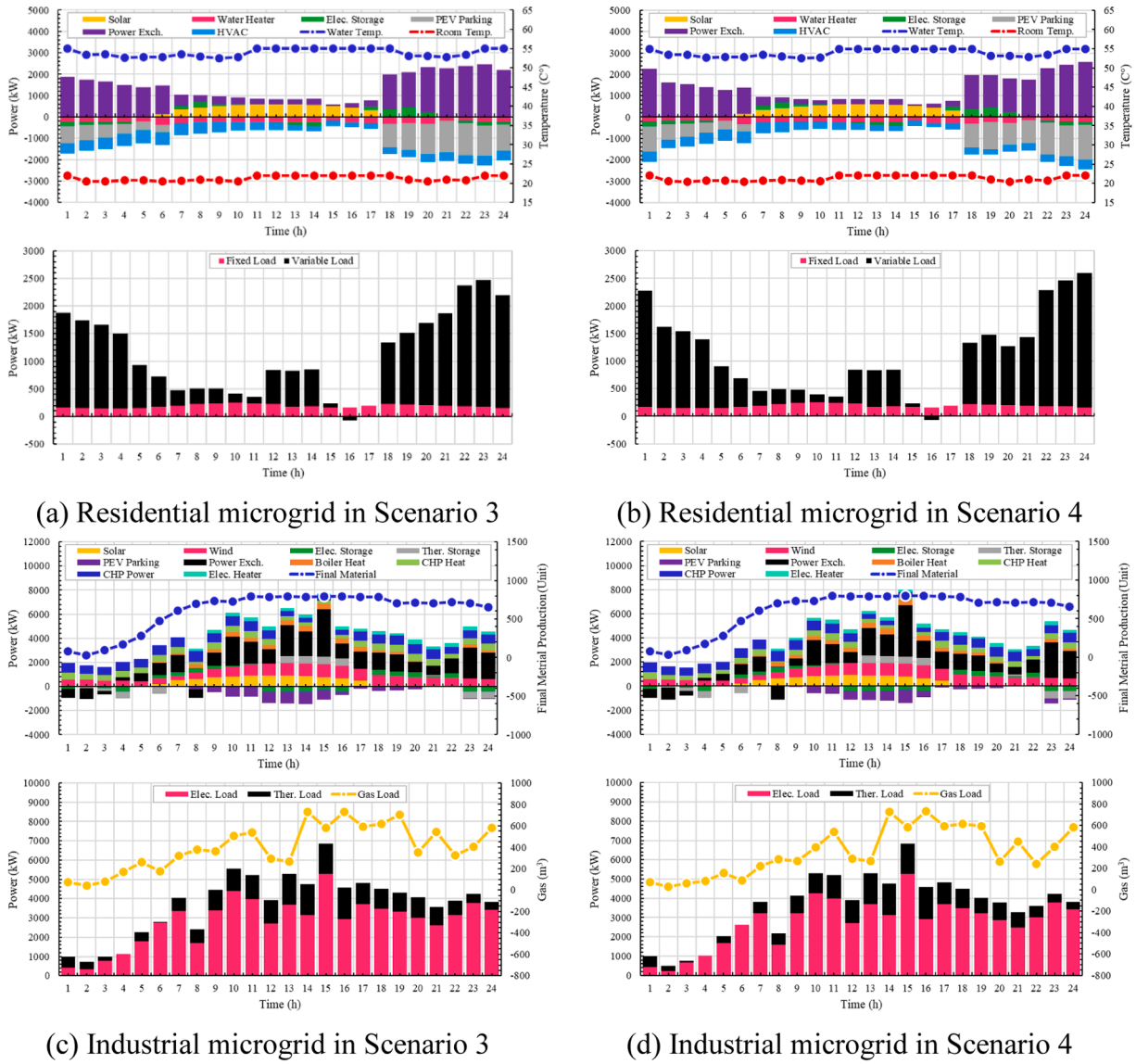

Fig. 11. Operational schedules obtained for microgrids in Scenarios 3 & 4.

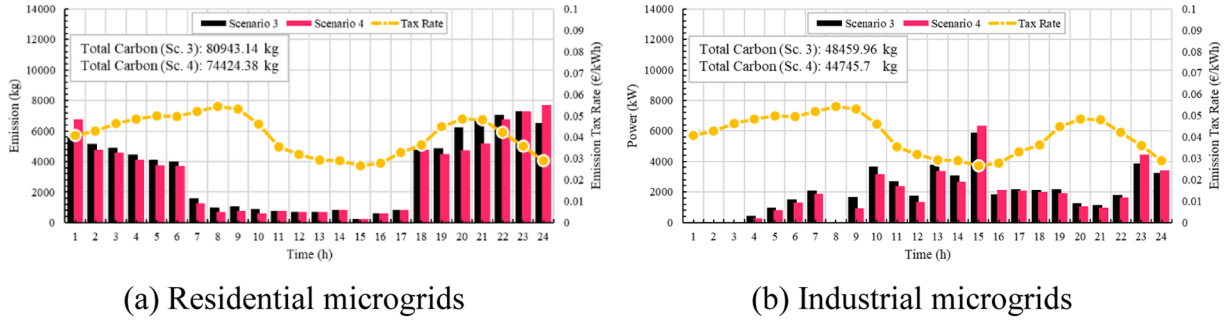

Fig. 12. Hourly carbon emissions of microgrids in Scenarios 3 & 4.

costs for the DNO, residential microgrids, and industrial microgrids by 5.46 %, 3.56 %, and 3.48 %, respectively. However, Figs. 13a and 13b demonstrate that during real-time operation, characterized by fluctuations in load demand and renewable power generation, agents employing the robust approach avoided reliance on the costly spot electricity market. Conversely, under Scenario 4's deterministic scheduling, agents participated in the spot market across all ten scenarios to address energy mismatches caused by these fluctuations. This analysis confirms that while robust scheduling increases upfront costs, it effectively mitigates additional expenses during real-time operation, ensuring resilience to uncertainties. Note that to simulate real-time operational uncertainties, 10 scenarios for each uncertain parameter, load demand, solar radiation, and wind speed, were generated using Gaussian, Beta, and Weibull distributions, respectively. These were

Table 8
Numerical outcomes derived from solving Scenario 5.

Agents	Day-Ahead Scheduling Costs (€)					Carbon Emissions (kg)
	Internal Technologies	Penalty for Deviating from Preferred Schedules	Exchange between DNO and Microgrids	Exchange between DNO and Upstream Network	Sum	
DNO	5981.33	-	-100761.82	92870.92	-1909.57	122586.04
Residential Microgrids	795.33	161.29	62877.77	-	63834.39	77077.5
Industrial Microgrids	927.56	210.09	37884.05	-	39021.7	46305.76
Total	7704.22	371.38	0	92870.92	100946.5	245969.3

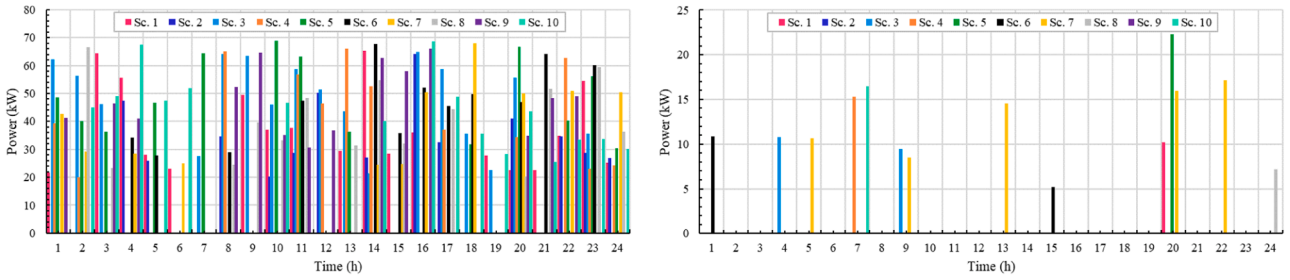

(a) Scenario 4 (Deterministic scheduling) (b) Scenario 5 (Robust scheduling)

Fig. 13. Impact of real-time operational uncertainties on day-ahead schedules.

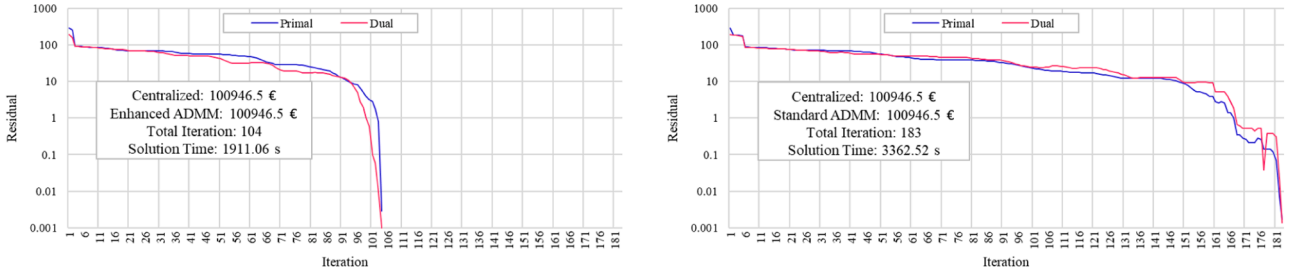

(a) Scenario 5 (Proposed ADMM) (b) Scenario 6 (Standard ADMM)

Fig. 14. Convergence analysis of the proposed and standard ADMM versions.

combined into 1000 scenarios, which were subsequently reduced to 10 representative scenarios using the ScenRed tool in GAMS.

Scenario 6 was subsequently solved using the same settings as Scenario 5, except that the link between the first and second layers employed the standard version of the ADMM algorithm instead of the proposed enhanced version. To evaluate performance, the proposed model was also optimized in a centralized manner, with an objective function minimizing the costs of all agents, enabling a direct comparison of results from both the standard and enhanced versions against the global optimal solution. Fig. 14a and 14b illustrate the convergence processes of the enhanced and standard ADMM versions, respectively. These figures display the primal and dual residuals at each iteration of the algorithm, where convergence is achieved when the difference between these values falls below a tolerance of 0.001.

The enhanced ADMM version converged in 104 iterations, requiring 1911.06 seconds, while the standard version required 183 iterations and 3362.52 seconds to converge. These findings demonstrate that the enhanced version, with logarithmic updates to the ADMM's penalty coefficient, achieved convergence in 79 fewer iterations, corresponding to a 43.16 % reduction in solution time. Furthermore, the operating cost for the entire system was identical across the enhanced, standard, and centralized optimization approaches, confirming that both ADMM versions reached the global optimal solution.

5. Conclusion

This study introduces a two-layer robust optimization framework based on an enhanced ADMM algorithm for day-ahead scheduling of emission-aware microgrids in renewable-rich smart grids. The proposed model effectively addresses critical challenges, including decentralized coordination, carbon emission reduction, and robust scheduling under uncertainties in renewable generation and load demand. The following key insights and numerical results were derived from the study:

- Incorporating carbon tax rates into the dynamic pricing mechanism achieved a 10.67 % reduction in total emissions while causing only a modest 4.7 % increase in daily operating costs, highlighting the effectiveness of proposed pricing mechanism in fostering environmentally sustainable operations.
- The activation of energy storage systems and V2G provider technologies, compared to the case where they are absent, led to a 15.67 % reduction in operational costs and a 15.2 % decrease in carbon emissions, highlighting the significant flexibility and decarbonization potential of these technologies within residential and industrial microgrids.
- Implementing robust scheduling under uncertainty resulted in an average 4.5 % increase in day-ahead costs but successfully

eliminated reliance on costly real-time markets, thereby ensuring both cost-effective and resilient operations.
- The proposed enhanced ADMM algorithm demonstrated a 43.16 % reduction in convergence time compared to the standard version, confirming its effectiveness in expediting agent coordination in day-ahead electricity markets. This improvement underscores its potential for practical implementation in decentralized energy systems, where computational efficiency is critical.

Overall, the results emphasize the potential of leveraging distributed optimization techniques and flexible resources to align operational strategies with economic and environmental objectives. Future research could extend this framework to multi-energy systems, incorporating interactions with gas and heat networks to address broader decarbonization goals. Furthermore, the integration of advanced forecasting methods and real-time adaptive mechanisms could enhance the framework's applicability in dynamic operational environments.

CRediT authorship contribution statement

Yali Wang: Writing – original draft, Software, Methodology, Investigation, Conceptualization. **Zeyi Fan:** Writing – original draft, Validation, Supervision, Conceptualization. **Yahya Z. Alharthi:** Writing – original draft, Visualization, Software, Methodology. **Shoujun Huang:** Writing – original draft, Formal analysis, Data curation. **Seyed Amir Mansouri:** Software, Methodology, Conceptualization.

Declaration of competing interest

The authors declare that they have no known competing financial interests or personal relationships that could have appeared to influence the work reported in this paper.

Acknowledgements

The research is supported by the National Social Science Fund of China (23BJY092), Humanities and Social Sciences Foundation of Ministry of Education of China (21YJC790053), and Anhui Provincial Natural Science Foundation (2208085MG191).

Data availability

Data will be made available on request.

References

Ali, Z. M., Al-Dhaifallah, M., Alkhalaf, S., Alaas, Z., & Jamali, F. (2023). Optimal planning and design of a microgrid with integration of energy storage and electric vehicles considering cost savings and emissions reduction. *Journal of Energy Storage, 71*, Article 108049. https://doi.org/10.1016/j.est.2023.108049

Alomoush, M. I. (2020). Optimal combined heat and power economic dispatch using stochastic fractal search algorithm. *Journal of Modern Power Systems and Clean Energy, 8*(2), 276–286. https://doi.org/10.35833/MPCE.2018.000753

Alrasheedi, A. F., Alnowibet, K. A., & Alshamrani, A. M. (2024). A smart predict-and-optimize framework for microgrid's bidding strategy in a day-ahead electricity market. *Electric Power Systems Research, 228*, Article 110016. https://doi.org/10.1016/j.epsr.2023.110016

Bolurian, A., Akbari, H., & Mousavi, S. (2022). Day-ahead optimal scheduling of microgrid with considering demand side management under uncertainty. *Electric Power Systems Research, 209*, Article 107965. https://doi.org/10.1016/j.epsr.2022.107965

Cagnano, A., De Tuglie, E., & Mancarella, P. (2020). Microgrids: overview and guidelines for practical implementations and operation. *Applied Energy, 258*, Article 114039. https://doi.org/10.1016/j.apenergy.2019.114039

Chen, Y., Li, Z., Yu, S. S., Liu, B., & Chen, X. (2024). A profitability optimization approach of virtual power plants comprised of residential and industrial microgrids for demand-side ancillary services. *Sustainable Energy, Grids and Networks, 38*, Article 101289. https://doi.org/10.1016/j.segan.2024.101289

Costanzo, V., Nocera, F., Detommaso, M., & Evola, G. (2024). Decarbonizing cities through electrification: A strategic study for densely built residential districts in Southern Italy. *Sustainable Cities and Society, 113*, Article 105651. https://doi.org/10.1016/j.scs.2024.105651

Fuchs, I., Rajasekharan, J., & Cali, Ü. (2024). Decentralization, decarbonization and digitalization in swarm electrification. *Energy for Sustainable Development, 81*, Article 101489. https://doi.org/10.1016/j.esd.2024.101489

Herding, R., Ross, E., Jones, W. R., Charitopoulos, V. M., & Papageorgiou, L. G. (2023). Stochastic programming approach for optimal day-ahead market bidding curves of a microgrid. *Applied Energy, 336*, Article 120847. https://doi.org/10.1016/j.apenergy.2023.120847

Hossain Lipu, M. S., Ansari, S., Miah, M. S., Hasan, K., Meraj, S. T., Faisal, M., Jamal, T., Ali, S. H. M., Hussain, A., Muttaqi, K. M., & Hannan, M. A. (2022). A review of controllers and optimizations based scheduling operation for battery energy storage system towards decarbonization in microgrid: challenges and future directions. *Journal of Cleaner Production, 360*, Article 132188. https://doi.org/10.1016/j.jclepro.2022.132188

Hui, H., Bao, M., Ding, Y., Yan, J., & Song, Y. (2023). Probabilistic integrated flexible regions of multi-energy industrial parks: conceptualization and characterization. *Applied Energy, 349*, Article 121521. https://doi.org/10.1016/j.apenergy.2023.121521

Hwang Goh, H., Shi, S., Liang, X., Zhang, D., Dai, W., Liu, H., Yuong Wong, S., Agustiono Kurniawan, T., Chen Goh, K., & Leei Cham, C. (2022). Optimal energy scheduling of grid-connected microgrids with demand side response considering uncertainty. *Applied Energy, 327*, Article 120094. https://doi.org/10.1016/j.apenergy.2022.120094

Ifaei, P., Esfehankalateh, A. T., Na, J., & Yoo, C. (2025). Optimal hybrid renewable microgrids via energy demand control using media platforms in South Korea. *Sustainable Cities and Society, 118*, Article 106027. https://doi.org/10.1016/j.scs.2024.106027

Jin, G., Huang, K., Yang, C., & Xu, J. (2024). Day-ahead scheduling of microgrid with hydrogen energy considering economic and environmental objectives. *Energy Reports, 12*, 1303–1314. https://doi.org/10.1016/j.egyr.2024.07.036

Li, H., Wu, Q., Yang, L., Zhang, H., & Jiang, S. (2024). Distributionally robust negative-emission optimal energy scheduling for off-grid integrated electricity-heat microgrid. *IEEE Transactions on Sustainable Energy, 15*(2), 803–818. https://doi.org/10.1109/TSTE.2023.3306360

Ma, W. J., Wang, J., Gupta, V., & Chen, C. (2018). Distributed energy management for networked microgrids using online ADMM with regret. *IEEE Transactions on Smart Grid, 9*(2), 847–856. https://doi.org/10.1109/TSG.2016.2569604

Mansouri, S. A., Nematbakhsh, E., Ramos, A., Tostado-Véliz, M., Aguado, J. A., & Aghaei, J. (2024). A robust ADMM-enabled optimization framework for decentralized coordination of microgrids. *IEEE Transactions on Industrial Informatics*, 1–10. https://doi.org/10.1109/TII.2024.3478274

Mansouri, S. A., Nematbakhsh, E., Ramos, A., Tostado-Véliz, M., Aguado, J. A., & Aghaei, J. (2025). A robust ADMM-enabled optimization framework for decentralized coordination of microgrids. *IEEE Transactions on Industrial Informatics, 21*(2), 1479–1488. https://doi.org/10.1109/TII.2024.3478274

Mansouri, S. A., Rezaee Jordehi, A., Marzband, M., Tostado-Véliz, M., Jurado, F., & Aguado, J. A. (2023). An IoT-enabled hierarchical decentralized framework for multi-energy microgrids market management in the presence of smart prosumers using a deep learning-based forecaster. *Applied Energy, 333*, Article 120560. https://doi.org/10.1016/j.apenergy.2022.120560

Nawaz, A., Zhou, M., Wu, J., & Long, C. (2022). A comprehensive review on energy management, demand response, and coordination schemes utilization in multi-microgrids network. *Applied Energy, 323*, Article 119596. https://doi.org/10.1016/j.apenergy.2022.119596

Neri, A., Butturi, M. A., Lolli, F., & Gamberini, R. (2023). Inter-firm exchanges, distributed renewable energy generation, and battery energy storage system integration via microgrids for energy symbiosis. *Journal of Cleaner Production, 414*, Article 137529. https://doi.org/10.1016/j.jclepro.2023.137529

Perwez, U., Rasool, M. H., Aziz, I., & Zia, U. (2025). UBEM-SER: role of sufficiency, efficiency and renewable in the decarbonization of commercial building stock at city scale. *Sustainable Cities and Society, 121*, Article 106214. https://doi.org/10.1016/j.scs.2025.106214

Ranjbar, G. A., Simab, M., Nafar, M., & Zare, M. (2024). Day-ahead energy market model for the smart distribution network in the presence of multi-microgrids based on two-layer flexible power management. *International Journal of Electrical Power & Energy Systems, 155*, Article 109663. https://doi.org/10.1016/j.ijepes.2023.109663

Sharma, P., Dutt Mathur, H., Mishra, P., & Bansal, R. C. (2022). A critical and comparative review of energy management strategies for microgrids. *Applied Energy, 327*, Article 120028. https://doi.org/10.1016/j.apenergy.2022.120028

Shen, H., Zhang, H., Xu, Y., Chen, H., Zhang, Z., Li, W., Su, X., Xu, Y., & Zhu, Y. (2024). Two stage robust economic dispatching of microgrid considering uncertainty of wind, solar and electricity load along with carbon emission predicted by neural network model. *Energy, 300*, Article 131571. https://doi.org/10.1016/j.energy.2024.131571

Silva-Rodriguez, L., Sanjab, A., Fumagalli, E., & Gibescu, M. (2024). Light robust co-optimization of energy and reserves in the day-ahead electricity market. *Applied Energy, 353*, Article 121982. https://doi.org/10.1016/j.apenergy.2023.121982

Tsaousoglou, G., Giraldo, J. S., & Paterakis, N. G. (2022). Market Mechanisms for Local Electricity Markets: A review of models, solution concepts and algorithmic techniques. *Renewable and Sustainable Energy Reviews, 156*, Article 111890. https://doi.org/10.1016/j.rser.2021.111890

Venkatesan, K., Gouda, P. K., Rath, B. B., & Krishnamoorthy, M. (2024). Optimal day-ahead scheduling of microgrid equipped with electric vehicle and distributed energy resources: SFO-CSGNN approach. *Journal of Energy Storage, 102*, Article 113933. https://doi.org/10.1016/j.est.2024.113933

Wang, J., Shao, Z., Wu, J., & Wu, L. (2024). Day-ahead strategic bidding of multi-energy microgrids participating in electricity, thermal energy, and hydrogen markets: A

stochastic bi-level approach. *International Journal of Electrical Power & Energy Systems, 163*, Article 110319. https://doi.org/10.1016/j.ijepes.2024.110319

Wang, Y., Zheng, Y., & Yang, Q. (2023). Day-ahead bidding strategy of regional integrated energy systems considering multiple uncertainties in electricity markets. *Applied Energy, 348*, Article 121511. https://doi.org/10.1016/j.apenergy.2023.121511

Wu, Y., Huang, S., Alharthi, Y. Z., & Wang, Y. (2025). Market scheduling of emission-aware smart prosumers in smart grids: A multi-objective bi-level approach. *Applied Energy, 389*, Article 125745. https://doi.org/10.1016/j.apenergy.2025.125745

Xie, X., & Sun, Y. (2022). A piecewise probabilistic harmonic power flow approach in unbalanced residential distribution systems. *International Journal of Electrical Power & Energy Systems, 141*, Article 108114. https://doi.org/10.1016/j.ijepes.2022.108114

Xu, Y. P., Liu, R. H., Tang, L. Y., Wu, H., & She, C. (2022). Risk-averse multi-objective optimization of multi-energy microgrids integrated with power-to-hydrogen technology, electric vehicles and data center under a hybrid robust-stochastic technique. *Sustainable Cities and Society, 79*, Article 103699. https://doi.org/10.1016/j.scs.2022.103699

Xu, Y., Ye, S., Qin, Z., Lin, X., Huangfu, J., & Zhou, W. (2023). A coordinated optimal scheduling model with Nash bargaining for shared energy storage and multi-microgrids based on two-layer ADMM. *Sustainable Energy Technologies and Assessments, 56*, Article 102996. https://doi.org/10.1016/j.seta.2022.102996

Yan, R., & Xu, Y. (2023). A data-driven method for microgrid bidding optimization in electricity market. *Energy Conversion and Economics, 4*(4), 276–286. https://doi.org/10.1049/enc2.12093

Zhang, P., Mansouri, S. A., Rezaee Jordehi, A., Tostado-Véliz, M., Alharthi, Y. Z., & Safaraliev, M. (2024). An ADMM-enabled robust optimization framework for self-healing scheduling of smart grids integrated with smart prosumers. *Applied Energy, 363*, Article 123067. https://doi.org/10.1016/j.apenergy.2024.123067

Zhong, X., Zhong, W., Liu, Y., Yang, C., & Xie, S. (2022). Optimal energy management for multi-energy multi-microgrid networks considering carbon emission limitations. *Energy, 246*, Article 123428. https://doi.org/10.1016/j.energy.2022.123428

Zou, Y., Xu, Y., & Zhang, C. (2023). A risk-averse adaptive stochastic optimization method for transactive energy management of a multi-energy microgrid. *IEEE Transactions on Sustainable Energy*, 1–12. https://doi.org/10.1109/TSTE.2023.3240184